Atomistic resolution structure and dynamics of lipid bilayers in simulations and experiments

O. H. Samuli Ollila[1,*]
[1]Aalto University
(Dated: November 12, 2015)

Recent progress in the analysis of lipid bilayer atomistic resolution structure and dynamics using combination of robust experimental data and molecular dynamics simulations is reviewed. The focus is on order parameters and spin relaxation times measured with NMR and on form factors measured with SAXS and SANS for phosphatidylcholine lipid bilayers. The experimental observables are chosen since these experiments are robust, well understood, highly reproducible and the connection between raw data and simulations is straightforward. Also the comparison between simulations and these observables is bidirectionally useful; it will quantitatively measure the quality of the simulation model respect to the reality, and if the quality is sufficient, the simulations give structural interpretation for the experimental data. Significant advance of molecular dynamics simulation models is that the same simulation model can be simultaneously compared to all of this parameters. If satisfactory agreement is found, it is highly likely that the model represents the reality due to the large amount of reproduced independent experimental parameters. In this case all the mentioned experiments would be simultaneously interpreted with the same model. Phosphatidylcholine lipids are chosen since large portion of model membrane studies have been focused on this lipid, producing enough experimental and simulation data to draw comprehensive picture on the level of understanding atomistic resolution structure and dynamics. We conclude that the acyl chain region structure and its changes are generally well described in simulations of lipid bilayers, in contrast to the glycerol backbone and choline. Also cation binding is significantly overestimated by several models.

INTRODUCTION

1.Citations missing Atomistic resolution structure and dynamics of lipid bilayers has been studied with wide range of techniques for many decades motivated mainly by their presence and important role in biological systems [1**?** –5]. Lipid bilayers play direct or indirect role in several physiological and pathological molecular scale processes [6**?** , 7]. To fully understand these processes the atomistic and molecular level understanding of lipids is required. Since atomistic resolution studies are extremely difficult for biological membranes, simplified lipid-only systems are often used [**?**]. The biological relevance of these model systems is supported, e.g. by similar NMR order parameters mesured from living cells, lipid extracts and model systems [**?**].

The most detailed information about lipid bilayer atomistic resolution structure and dynamics has been achieved with various Nuclear Magnetic Resonance (NMR) and scattering techiques [2–5, 8–10]. The first one giving direct information on structures sampled by individual lipid molecules [2**?** –4] and the latter one giving complementary information on average bilayer properties, like e.g. area per lipid or bilayer thickness [5, 8–10]. Both techniques give robust, accurate and reproducible quantities related to the strucuture and dynamics. However, for structural and dynamical interpretation both techniques need to model experimental data to produce the measured quantities [2–5, 8–10].

On the other hand, remarkable progress in hardware and software allows to routinely perform classical atomistic resolution molecular dynamics (MD) simulations of lipid bilayer with duration of tens or hundreds nanoseconds. Ideally the molecules are sampling realistic conformations with realistic speed in these simulations. This can be verified by calculating directly measurable quantities from simulations and comparing these to experimental values. Here we review such comparisons for different experimental observables: C–H bond order parameters, spin relaxation times and form factor. The first and second parameters are measured with NMR. Hence, they represent to structure and dynamics sampled by individual lipid molecules, respectively. The third quantitiy is obtained from elastic X-ray or neutron scattering experiments and encodes the overall structural bilayer properties.

The order parameters and spin lattice relaxation times have been compared between simulations and experiments for validation and interpretation since the early days of lipid MD simulations [11, 12]. On the other hand, scattering form factors for lipid bilayers have been replacing the comparisons of simulations to the experimental area per molecule during the last decade since form factor is directly measurable quantity while area per molecule value depends on model used to analyze the scattering data [5].

If an atomistic resolution model reproduces all the above mentioned experimental parameters, i.e. order parameters, spin relaxation rates and form factor, the simulation can be considered as an ultimate model giving interpretation for all these experiments simulatenously. In addition, it would be the correct atomistic resolution representation of the system with high probability since it reproduces large amount of indepentedly measured experimental parameters simultaneously. Thus, usage of the model for further specific questions and applications would be well justified.

Here we review recent studies comparing the order parameters, spin relaxation rates and scattering form factors between experiments and simulations in order to quantify the quality of simulation models and interpret the experiments. Also relevat techical details on experimental data and simulation analysis is reviewed. We focus on phosphatidylcholine lipid bilayers due to most comprehensive available datasets for both, simu-

lations and experiments. However, the basic ideas of the approach is valid also for other lipids and surfactants and there is also data and literature available [**?**]. We also discuss the observed structural changes of lipids induced by external conditions and their relation, e.g. to ion partition. We pay special attention on the accuracy and usability of the NMR order parameter data which is often underestimated in the literature, especially for the glycerol backbone and choline regions.

The general conclusion from the review is that the hydrophopic acyl chain region is well described in simulation models and the atomistic resolution interpretation of experiments has been successfull for this region. However, the glycerol backbone and choline regions are less well described in simulation models which may question their usability in studies where this region is important.

The structural details of the these segments are potentially relevant in several biochemical applications of atomistic resolution lipid bilayer simulations. For example, interactions between lipid bilayer with ions, drug molecules or proteins may be dependent on the detailed headgroup structure. Due to the large variation of lipid headgroups present in biological systems, its chemical details are most likely important at least for some physiological processes. One goal of this review is to demonstrate how model quality can be estimated to minimize possibility of artificial conclusions made from simulation studies.

C-H BOND ORDER PARAMETERS AS ATOMISTIC RESOLUTION STRUCTURAL MEASURE

2.The text should be close to final. Figures should be improved.

Definition and properties of C-H bond order parameter

In lipid bilayer systems the order parameter of a hydrocarbon C–H vector is typically defined as

$$S_{\mathrm{CH}} = \frac{1}{2}\langle 3\cos^2\theta - 1\rangle, \qquad (1)$$

where the angle brackets denote an ensemble average over the sampled conformations, and θ is the angle between the C–H bond and the membrane normal. The numerical values of order parameters vary between $-\frac{1}{2} < S_{\mathrm{CH}} < +1$ depending on the sampled θ distribution. The definition is motivated by its connection to the dipolar and quadrupolar splitting measured with ^{1}H-^{13}C and ^{2}H NMR techniques, respectively. The functional form comes from the fundamental theory of interactions between spin systems which gives a connection between average molecules orientations and NMR measurables [13].

If the sampled distribution of θ for a C–H bond are known, the order parameter can be straighfowardly calculated from Eq. 1. However, the sampled θ distribtions cannot be uniquely determined from the known order parameter. Thus the experimental order parameter values gives a set of conditions which the structural molecular model (more specifically the C–H bond vectors of the model) has to fulfill, but the experimental order parameters alone cannot be used to uniquely resolve the structure. The same applies practically to all experimental parameters used in biomolecular structure determination.

Atomistic resolution molecular dynamic simulations naturally produces the sampled structures and the calculated θ distributions can be substituted into Eq. 1 to calculate the order parameters. If and only if the experimental order parameters are reproduced, the sampled structures can be considered as a realistic atomistic resolution representation and used to interpretate experimental order parameters. Before MD simulations were feasible for such usage, other models have been used for this interpretation [14–21]. It is important to note, however, that reproduction of the order parameters does not absolutely guarantee that the sampled structures are correct since several structural models can produce the same order parameters, in principle. Significant advance of the MD models compared to the traditional models is that the same MD structures can be straightforwardly compared to other experimental observables in addition to order parameters, like ^{31}P chemical shift anisotropy [22], ^{31}P-^{13}C dipolar couplings [23], spin relaxation data [24] and scattering data [25]. The comparisons of the same model to the various independently measured experimental observables significantly reduces the possibility of getting unrealistic structures.

The probability for unrealistic structures is further reduced by the large amount of experimentally available order parameter values. As discussed in this review, the order parameters can be measured with high accuracy for each C–H pair of a lipid molecule in a liquid crystalline bilayer [2, 3, 26–30]. Also the signs [20, 27, 31] and stereospecifity of C–H segments in the same carbon (*forking*) [27–29, 32–34] are experimentally available. Consequently, a realistic atomistic resolution model, for example, for POPC molecule (see Fig. 1 B)) in liquid crystalline bilayer has to reproduce 82 experimental order parameter values. If these parameters are not reproduced for certain segments, the model deficiencies are easy to localize since the segmental order parameter is a very local quantity depending only on the position of two atoms (C-H pair). This is an advance over several other accurately measured NMR quantities depending on the position of several atoms [22, 23], thus complicating the localization of strucutral differences in the case of disagreement between model and experiments.

Experimental order parameter data for single component lipid bilayers are easily available in the literature [29, 30, 51–56]. The amount of data, especially from ^{13}C NMR, has been also increasing of late [29, 51, 52, 55, 56]. Further, changes of order parameters for all lipid segments have been measured various experimental different conditions, like temperature [**?**], hydration level [28, 37, 57, 58] and in the presense of ions, charged objects [36, 59–61], cholesterol [29, 56, 62, 63] and proteins [55, 64, 65]. The comparison of order parameter responses between experiments and simulations has not been much utilized so far. Thus we will exemplify its potential by showing the effect of Na^+ ions on choline order parameters

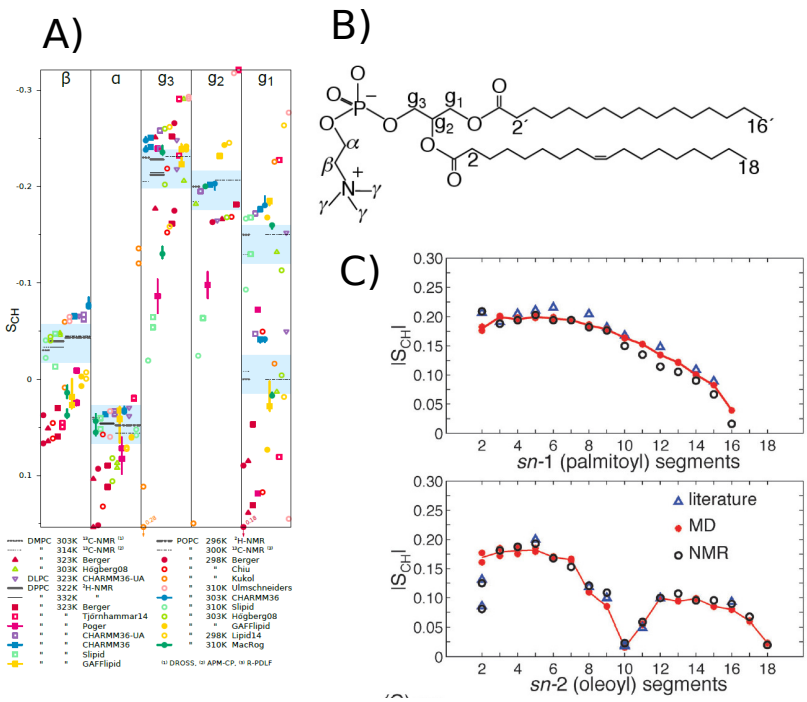

FIG. 1: A) Order parameters from simulations and experimens for phosphatidylcholine headgroup and glycerol backbone segments adapted from Botan et al. [30]. The blue shaded regions show the subjective sweetspots where the simulation data should fall to agree with experiments, based on estimated quantitative accuracy of order parameter measurements by Botan et al. B) Chemical structure of 1-palmitoyl-2-oleoylphosphatidylcholine (POPC). C) Order parameters $|S_{\mathrm{CH}}|$ for POPC acyl chains from ^{1}H-^{13}C NMR at 300K (black dots) [29], from ^{2}H NMR at 300K (blue triangles, literature) [17, 35] and from MD simulations at 298K (red dots) [29]. The experimental values shown in A): DMPC 303 K [27], DMPC 314 K [28], DPPC 322 K [15], DPPC 323 K [36], POPC 296 K [37], and POPC 300 K [29]. The force fields in A): Berger [38], Hogberg08 [39], Poger [40], Ulmschneiders [41], Kukol [42], Chiu [43], CHARMM36 [44], GAFFlipid [45], Slipid [46], MacRog [47], Tjörnhammar14 [48], Lipid14 [49], CHARMM36-UA [50]. The interactive version of this figure is available at https://plot.ly/∼HubertSantuz/72/lipid-force-field-comparison/.

and its relation to ion partition in simulations [66] and experiments [36, 59–61].

In this work we discuss only order parameters obtained from multilamellar samples, as they are the closest experimental analogue to MD simulations with periodic boundary conditions. We do not discuss order parameters measured for other type of samples, such as, e.g. bicelles [67–69], or indirect measurements by using, e.g. relaxation data [70] since the comparison to the standard simulation setup is less straightforward.

Order parameters from ^{2}H NMR experiments

The absolute values of order parameters are connected to the quadrupolar splitting $\Delta\nu_Q$ in ^{2}H NMR experiments through the equation

$$|S_{\mathrm{CD}}| = \frac{4}{3}\frac{h}{e^2 qQ}\Delta\nu_{\mathrm{Q}}, \tag{2}$$

where e is the elementary charge, Q is the deuteron quadrupole moment and h is the Planck's constant. The parameter q is related to the largest electric field gradient and in practise its value is not known; therefore the static quadrupolar coupling constant $\frac{e^2qQ}{h}$ is defined, and its value measured

for different compounds in their solid state ($\Delta\nu_Q$ measurement from the system where order parameter is known to be 1). In C-D order parameter measurements for lipids, it is typical to use the value measured for different alkenes, $\frac{e^2qQ}{h}$=170 kHz. The relation between order parameters and quadrupolar splittings then becomes $S_{\mathrm{CD}} = 0.00784 \times \Delta\nu_{\mathrm{Q}}$. This relation is useful as many publications report only the quadrupolar splittings. For a review and more accurate description see the work of Seelig [26].

For ^2H NMR measurements the CH_2 segments have to be labeled with deuterium. This can be done specifically for a certain segment or for the several segments simultaneously [3, 4, 53]. In the first case, it is known that the measured order parameter (quadrupolar splitting) is related to the labeled segment. In the latter case several order parameters (quadrupolar splittings) are measured which arise from all the labeled segments, however, it is not known which order parameter belongs to which CH_2 segment. Majority of the ^2H NMR data in the literature are measured using samples with perdeuterated acyl chains [53, 54] while also order parameter data from specifically deuterated lipids are available for several lipid types in various conditions [14, 16, 17, 32, 33, 36, 57, 59, 61, 63–65].

Order parameters from ^{13}C NMR experiments

The order parameter can be related to the dipolar splitting $\Delta\nu_{\mathrm{CH}}$ from ^{13}C-^{1}H NMR experiment which is related to the effective dipolar coupling d_{CH} through a scaling factor depending on the used pulse sequence [27–29, 31]. The effective dipolar coupling d_{CH} is then connected to the absolute value of order parameter through equation

$$|S_{\mathrm{CH}}| = (\frac{D_{\mathrm{max}}}{2\pi})^{-1} d_{\mathrm{CH}}, \quad (3)$$

where $D_{\mathrm{max}} = \frac{\hbar\mu_0\gamma_h\gamma_c}{4\pi\langle r_{\mathrm{CH}}^3\rangle}$. r_{CH} is the C-H distance, μ_0 is the vacuum permittivity, and γ_h and γ_c are the gyromagnetic constants for ^{1}H and ^{13}C nuclei. In contrast to Eq. 2, all the parameters in Eq. 3 are in principle known. However, for the internuclear distance only the average $\langle r_{\mathrm{CH}}\rangle$ is known, but not the third moment $\langle r_{\mathrm{CH}}^3\rangle$. For this reason frequencies between 20.2-22.7 kHz have been used for $\frac{D_{\mathrm{max}}}{2\pi}$ [24, 27–29, 31, 71].

In contrast, specific labeling is not needed for ^{13}C NMR experiments due the natural abundance of ^{13}C. Labeling could be used though to enhance the signal for a specific segment of interest [72]. Order parameter measurements with ^{13}C NMR are 2D experiments, the chemical shift being in the first dimension and dipolar coupling in the second [27–29, 31]. The chemical shift depends on the local chemical environment and is different for each carbon segment. In the second dimension the dipolar coupling (order parameter) corresponding to each chemical shift value is measured, and its value can be connected, in principle, to each carbon segment by using the chemical shift value. This is straighforward for hydrocarbon segments in choline, glycerol backbone, close to the double bonds, and in the beginning and the end of acyl chains due to their distinct chemical shift values [27–29, 31, 56]. Challenges occur in the acyl chain region, where chemical shift values of different segments are very close to each other [27–29, 31, 56]. This issue has been solved by filtering the spectra by using partially deuterated lipids and data from simulations to help the assigment [29, 56].

Quantitative accuracy of experimental order parameter values

It must be stressed that ^{2}H NMR and ^{13}C NMR are fully independent experiments since the deuterium quadrupolar splitting $\Delta\nu_Q$ and the dipolar splitting d_{CH} are different physical observables. In addition, the prefactors connecting the observables to the order parameter (Eqs. 2 and 3) are independently measured. Further independent experiments are performed by measuring the ^{1}H-^{13}C dipolar couplings using different pulse sequences [27–29, 31] when the connection between dipolar splitting $\Delta\nu_{\mathrm{CH}}$ and effective dipolar coupling d_{CH} is different.

The measurements of quadrupole $\Delta\nu_Q$ and dipolar d_{CH} splittings are relatively accurate, especially for quadrupolar splitting. **3.How accurate exactly?** Thus the quantitative accuracy of measured order parameters is mainly determined by the prefactors connecting the splittings and order parameters in Eqs. 2 and 3. Since the prefactors are determined independently in ^{2}H and ^{13}C NMR measurements, the quantitative accuracy is best estimated by comparing the measured order parameter values.

These comparisons are done by several authors and generally show a very good agreement [27–30, 56]. Botan et al. collected literature values for PC lipid choline headgroup and glycerol backbone order parameters and concluded that order parameters would be known with the accuracy of $\pm$0.02 for these segments in purified PC lipid bilayer samples [30] which agrees with the estimate of Gross et al [27]. Based on this estimation Botan et al. suggested sweet spots where choline and glycerol backbone order parameters from simulations should range, see Fig. 1 A). Also acyl chain order parameters from different techniques are in good agreement when compared by several authors [27–29, 56], however the 0.02 accuracy might not be achieved for some segments.**4.Maybe specify to which ones?.** The comparison by Ferreira et al. [29] for POPC acyl chains is also shown in Fig. 1 C).

Qualitative accuracy of experimental order parameter values

When order parameter changes are measured with varying conditions, like temperature [14, 16, 63], hydration level [28, 37, 57, 58], presense of ions [36, 59–61], cholesterol [29, 56, 62, 63] or proteins [55, 64, 65], the prefactors connecting the order parameters and the measured couplings in Eqs. 2 and 3 can be considered to be unchanged. Therefore,

accuracy of the measured change is determined by the accuracy of the splitting measurement, in contrast to the prefactor discussed above. Here we refer to this as a qualitative accuracy. Due to the high resolution of splitting measurements, especially in ^{2}H NMR, the qualitative accuracy is much higher than the quantitative accuracy discussed in previous section.

The high qualitative accuracy of order parameter measurements is demonstrated in Figs. 2 and 3 showing the measured changes as a function of ion concetrations and hydration level, respectively. Systematically observed order parameter decrease of choline α and β segments due to penetrating positive charges [36, 59–61] from ^{2}H NMR are shown in Fig. 2 A). The quadrupole splittings reported in the original work [36] and corresponding order parameters are shown. The distinct quadrupolar splitting changes correspond to order parameter changes below 0.03 and 0.05 units for β and α, respectively. Systematically observed increase for choline β and α segments due to decreased hydration level are shown in Fig. 3. A similar increase is observed for different phosphatidycholine lipids in slightly different temperatures by different groups using both ^{2}H NMR [37, 57] and ^{13}C NMR [73]. The results demonstrate the systematic changes only slightly above 0.01 units can be detected also with ^{13}C NMR [73].

In conclusion, the order parameter changes can be measured with very high accuracy, thus even very small structural changes can be observed. Molecular models are necessary to analyze the measured changes to avoid overinterpretation from tiny changes observed in experiments. For example, high concentration of cholesterol induces measurable changes (less than 2 kHz) to the DPPC α and β quadrupolar splittings, however, the related structural changes are probably almost negligible [30, 62].

Signs of order parameters

^{2}H NMR [26] and standard ^{1}H-^{13}C NMR [27–29, 31] measure only the absolute value of order parameter. However, two different ^{1}H-^{13}C NMR techniques applied to eggPC [31] and DMPC [27, 31] allow also the measurement of the sign. The experiments report negative order parameters for almost all the segments, only α and γ are positive. Furthermore, the signs [20, 27, 31] and magnitudes [29, 30, 33] of choline headgroup and glycerol backbone order parameters are practically unaffected by the acyl tail contents of the bilayers. The results indicate that the order parameter signs for these segments can be assumed to be the same in all PC lipids in bilayer. On the other hand, positive signs for g_1, g_3 and C_2 have been reported by Aussenac et al. [67], which has led to some confusion in the simulation community [39, 74, 75]. However, these signs were not directly measured but extracted from the model used to interpret ^{2}H NMR order parameters from DMPC bicelles [67]. Thus, it is reasonable to conclude that order parameters are negative for all segments except for α and γ, as directly measured with ^{1}H-^{13}C NMR [20, 27, 31].

In measurements of order parameter changes with respect to varying conditions [14, 16, 28, 29, 36, 37, 55–65] only the absolute values are measured. However, the experiments are usually done by gradually changing the conditions and systematic order parameter responses are observed [29, 36, 37, 57–59, 73] (see also Figs. 2 and 3), indicating that sudden changes of sign do not occur. On the other hand, the large amount of bound positive charge may decrease the α carbon order parameter below zero as demonstrated by the spectra measured by Altenbach and Seelig [59] for POPC with high concetrations of $CaCl_2$, shown in Fig. 4.

Forking of order parameters

The order parameters for two C–H bonds in the same CH_2 segment are equal for the most segments in lipids [14, 16, 17, 27–29, 33]. However, this is not the case for g_1, g_3, and the C_2 carbon in the *sn*-2 chain segments in a fluid PC lipid bilayer as observed with both ^{2}H NMR [17, 32–34] and ^{1}H-^{13}C NMR techniques [27–29], see also Fig. 1. We call this phenomena *forking*, as done also previously to avoid confusion with splittings measured with NMR [30].

The forking has been studied in detail with ^{2}H NMR techniques by separately deuterating the R or S positions in CH_2 segments in order to assign order parameters to correct hydrogens [33, 34]. These studies also show that the forking arises from differently sampled orientations of the two C–H bonds, but not from two separate populations of lipid conformations [33, 34]. This means that the realistic atomistic resolution molecular model has to reproduce the forking correctly and the isomeric positions of hydrogens must be taken into account when calculating order parameters from simulations [30].

Order parameters from simulations

Since all the atom coordinates are available from molecular dynamics simulations trajectory, the order parameters can be calculated directly from the definition in Eq. 1. The ensemble average is taken over the time and all the molecules in simulation. The hydrogen positions can be generated post-simulationally for united atom simulations without explicit hydrogens by creating a trajectory with added hydrogens [30, 76], or by using equations to directly calculate order parameters [77, 78] based on heavy atoms positions and the known hydrocarbon geometries. The first approach is appropriate for accurate structural studies since it allows to analyse forking in contrast to the latter technique.

The difference in the analysis methods for the forked segments is most likely the reason for diverging choline and glycerol backbone order parameters reported for the same models by different authors [30, 79]. Also different order parameters for C–H segments attached to double bond are reported for the same model [76, 80] due to a bug in a widely-used version of the *g_order* program in the Gromacs package. The *g_order*

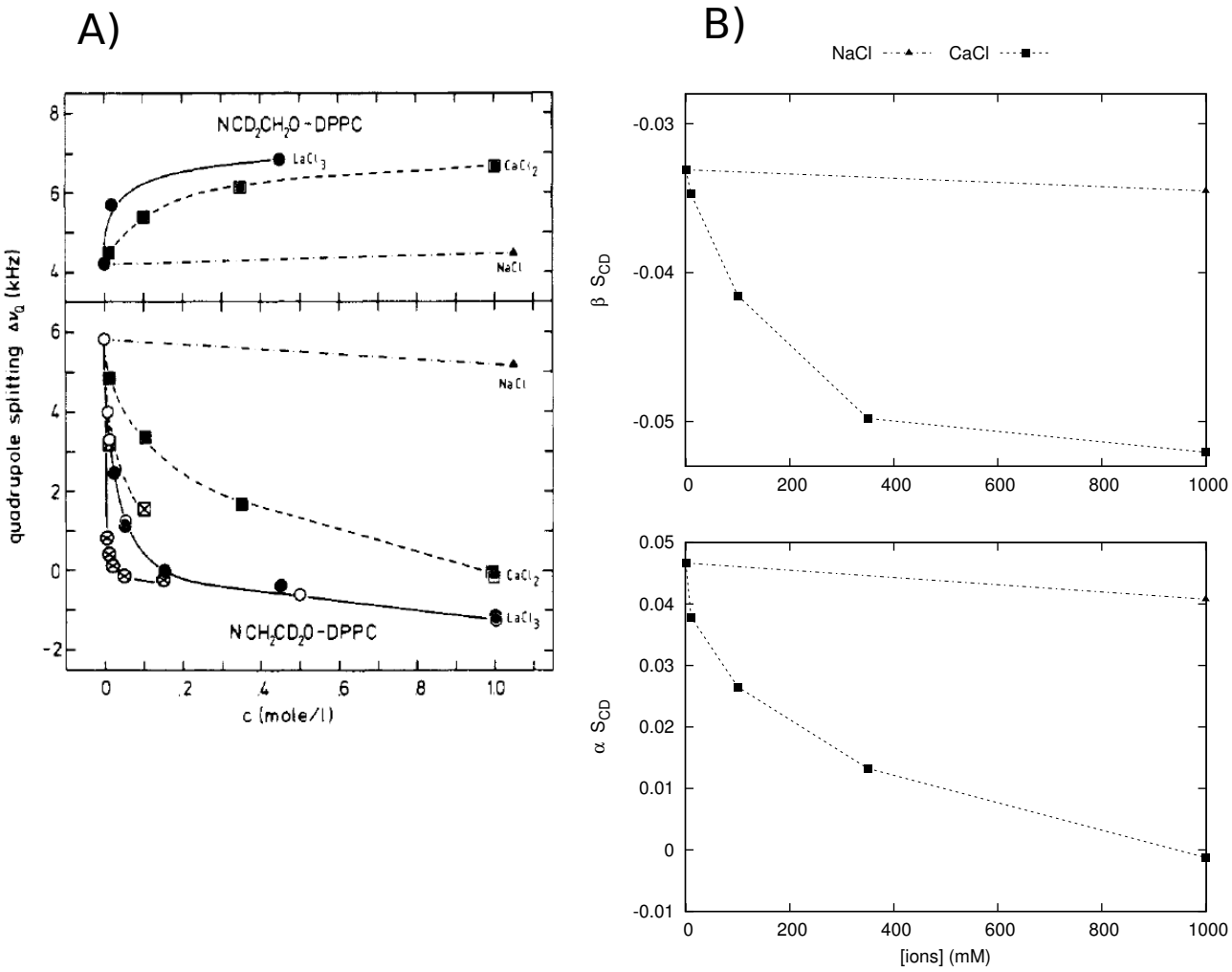

FIG. 2: A) Quadrupolar splittings of DPPC α and β segments as a function of different ion concetrations measured by Akutsu and Seelig with ^{2}H NMR [36]. B) The measured quadrupolar splittings with NaCl and $CaCl_2$ translated to order parameters ($S_{\rm CD} = 0.00784 \times \Delta\nu_{\rm Q}$). The negative sign for β order parameter is assigned according to more recent experiments [20, 27, 31] (see also Ref. [30] and Section 4). These changes were later shown to be consistent with the addition of different charges into the bilayer, and the electrometer concept was introduced to measure the amount of charge incorporated in the bilayer interface [36, 59–61].

program also prints -$S_{\rm CH}$, which is the most likely reason for the reported positive order parameters for acyl chains in some studies [81]. When these technical issues are taken into account, the different order parameters calculations from simulations are in good agreement.

The statistical error for order parameters is estimated by using the error of the mean for time blocks [76], independent simulations [79] and different lipids [30]. All these approaches yield a maximum error of $\sim \pm 0.01$.

It was recently pointed out that the sampling of individual dihedral angles might be very slow compared to the typical (100 ns) simulation timescales [82]. This result raises a question if the molecules sample the full phase phase during typical simulation time scales. On the other, another a recent study showed that the slowest rotational auto-correlation function observed (for g_1 segment) in the Berger model reached a plateau ($S^2_{\rm CH}$) after $\sim$200 ns and its relaxation was significantly too slow compared to NMR relaxation experiments [24]. This indicates that the typical simulation times are long enough for full conformational phase space sampling for the models with realistic dynamics [24].

Comparison between order parameters from simulations and experiments

The acyl chain order parameters are compared between simulations and experiments since the early days of lipid bilayer simulations [11, 38, 77, 83–92]. Good agreement has been generally found [22, 38–50]. except for the C_2 segment of the *sn-2* chain which has a low magnitude and significant forking in all PC lipids, in constrast to C_2 of the chain linked to *sn*-1 [14, 27–29, 32], for example see Fig. 1 C). This feature is, however, not analyzed or not reproduced for several

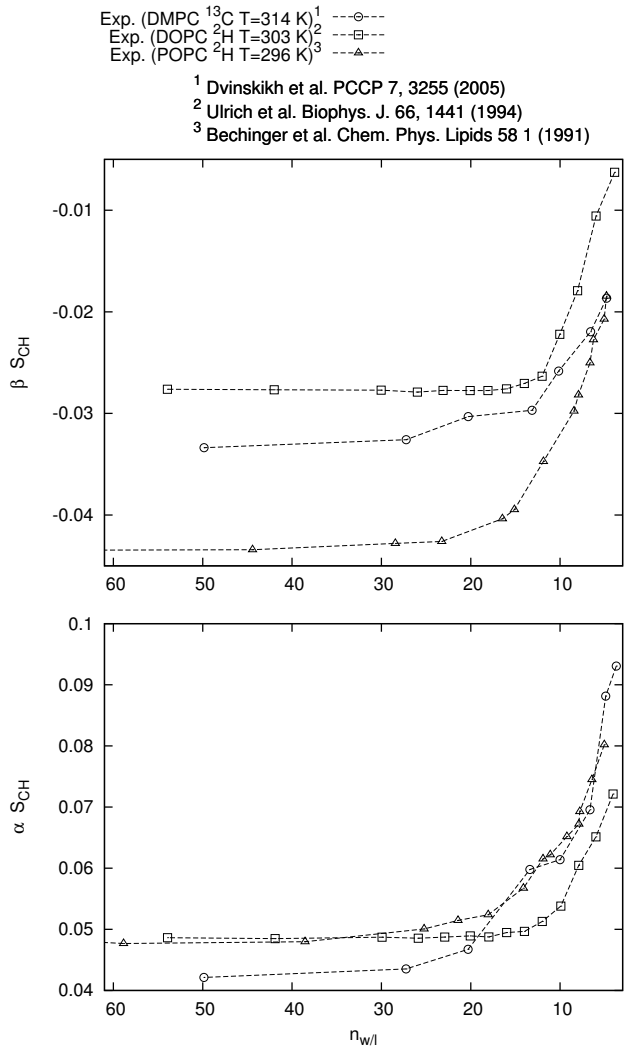

FIG. 3: Systematic increase of phosphatidylcholine α and β order parameters with decreasing hydration level, observed with both ^{2}H NMR [37, 57] and ^{13}C NMR [73]. The negative sign for β order parameter is assigned according to more recent experiments [20, 27, 31] (see also Ref. [30] and Section 4). The choline order parameter increase is related to the P-N vector tilting more parallel to the membrane plane [30] while relation between order parameter decrease and tilting more perpendicular has been suggested [61].

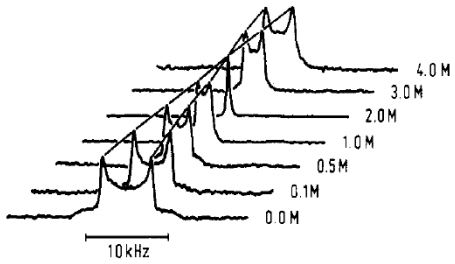

FIGURE 1: ^{2}H NMR spectra of coarse dispersions of POPC bilayers at various $CaCl_2$ concentrations (no NaCl). The lipid was deuterated at the α-segment ($-NCH_2CD_2OP-$). Measuring temperature, 40 °C.

FIG. 4: Quadrupolar splitting $\Delta\nu_Q$ for α segment in POPC as a function of $CaCl_2$ concentration measured by Altenbach and Seelig [59]. The splitting is related to the order parameter as $S_{\rm CD} = 0.00784 \times \Delta\nu_Q$. More recent studies show that the α order parameter is positive in the absense of $CaCl_2$ [20, 27, 31]. Thus, the most obvious interpertation is that the α order parameter decreases to zero when $CaCl_2$ concentration reaches 2.0M, and becomes increasingly negative with further addition of $CaCl_2$. Reprinted with permission from Altenbach and Seelig, Biochemistry, 23, 3913 (1984). Copyright 1984 American Chemical Society.

lipid models [22, 39, 41–43, 45–48, 93]. Some models report the small order parameter for C_2, but the forking is not reproduced correctly or analyzed [22, 44, 49, 93]. Among all studied force fields, the united atom CHARMM36 is closest to the experimental results [50].

Also acyl chain order changes with varying conditions are compared between simulations and experiments by several authors. Experimentally observed order parameter increase with cholesterol concentration [29, 63, 78, 94–96] and dehydration [58, 73] is observed also in simulations [29, 74, 78, 97–101], as well as the temperature induced order parameter decrease [63, 102]. A more careful comparison reveals, however, that the temperature and dehydration effects are slightly underestimated in simulations compared to experiments [74, 102]. Also cholesterol effects to DMPC bilayer are underestimated in the CHARMM36 model [99], while Slipids [100] and Amber Lipid14 [101] models show satisfactory agreement. The comparison of a Berger/Höltje [38, 103] based model to the extensive data set with various POPC/cholesterol mixtures shows good agreement with experiments for low cholesterol concetrations, however, the agreement gets worse for cholesterol concentration $\geq$ 34% [29]. A recent comparison of the Amber Lipid14 model to the same data shows signifincantly better agreement [101], also shown in Fig. 5. The orientation of cholesterol ring structure is reasonable in all models [29, 78, 99, 101], however, the cholesterol acyl chain exhibits too low order parameters in the Berger/Höltje [38, 103] based model and too much forking in Amber Lipid14 [101], while CHARMM36 reproduces experiments well [99].

The dip of the acyl chain order parameter profile due to double bonds is generally reproduced by different simulation models [29, 44, 45, 49, 50, 76, 80, 100, 104–112]. The particularly good agreement, often achieved for the oleyl chain in POPC bilayer with one *cis* double bond, is demonstrated in Fig. 1 C). Also the further order parameter decrease due to multiple double bonds (polyunsaturation) [76, 80, 104, 105, 107–109, 111, 112] is usually well reproduced, as demonstrated in Fig. 6 for Berger [38] based model with double bond description by Bachar et al. [80]. Also difference between *cis* and *trans* double bonds can be reproduced in MD

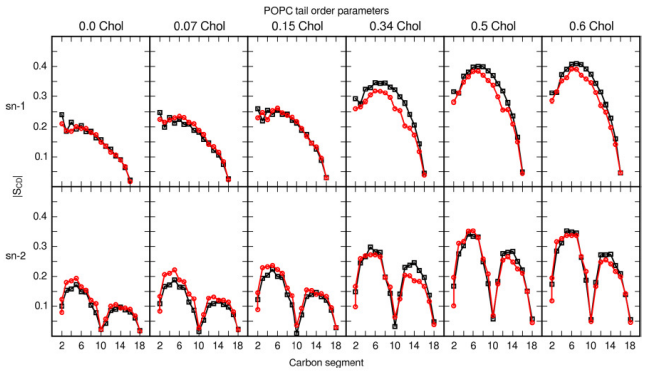

FIG. 5: Cholesterol effect on acyl chain order parameters compared between ? model [101] and experiments [29]. The agreement with experiments with this model is significanly better than Beger/Höltje based model compared by Ferreira et al. [29].

simulations [113].

In contrast to acyl chains, the glycerol backbone and choline order parameters are not routinely compared between simulations and experiments. In most comparisons the experimentally available signs, stereospecific labeling and high accuracy are not fully exploited [30, 39, 44, 45, 74, 79, 91, 116]. These issues were recently dicussed by Botan et al. who also compared order parameters between 13 different simulation models and experiments [30]. The results, shown also in Fig. 1 A), reveal significant differences between models and experiments, and none of the available models reproduces all order parameters within experimental error. On the other hand, experimentally observed choline order parameter increase and decrease with dehydration [37, 57, 73] and cation penetration [36, 59], respectively, were reproduced in simulations [30, 66]. However, especially the effect induced by Na^+ ion penetration is strongly overestimated in most models which arises most likely from an artificially high partition coefficient [66], as also demonstrated in Fig. 7. The effect of cholesterol on glycerol backbone and choline was overestimated by the Berger/Höltje based model while CHARMM36 and MacRog performed better [30].

In conclusion, the acyl chain order parameters and their qualitative changes are generally well described in atomistic MD models, except for C_2 segment in *sn*-2. However, all models have difficulties with varying severity to describe the glycerol backbone and choline order parameters.

Interplay between simulations and NMR order parameters: Validation and interpretation

Since the acyl chain order parameters from MD models generally agree with experiments for single component lipid bilayers in full hydration, the conformations sampled in simulations can be considered as realistic atomistic resolution structures for the acyl chains (except for the C_2 segment in the *sn*-2 chain). As also the acyl chain rotational dynamics has correct order of magnitude (see Section 4), the dynamical nature of hydrophopic region of lipid bilayers seen in simulation videos can be considered as a realistic representation. This is significant advancement to the traditional static structural models [14, 17, 19, 117]. Since lipid bilayers are considered as a simple models for cell- and other biological membranes, the intuitive understanding of their dynamical nature has a significant impact on biomembrane physics and chemistry.

Also more detailed structural interpretation has been succesfull for acyl chain region, especially for order parameter decrease due to *cis* double bonds [76, 80, 108, 109, 118–120]. From NMR experiments alone it was not possible to judge if the order parameter decrease arises from reduced chain order or the changes in average θ angle in Eq. 1 [119**?** , 120]. The interpretation of NMR experiments with the help of MD simulations and other calculations revealed that double bonds, indeed, decrease the chain order due to the flexible dihedral potentials next to the rigid double bonds [76, 80, 108, 109, 118–120].

The acyl chain order parameter increase and related bilayer thickening with cholesterol concentration [29, 101**?**], dehydration [74, 97] and reduced temperature [102] are qualitatively reproduced by simulations giving intuitive visualizations for these effects. However, the order parameter changes are often under- or overestimated [29, 74, 99, 101**?** , 102], thus it is not clear how well the models can be used for atomistic resolution intepretation of these changes. For example, delicate lipid-cholesterol interactions are known to induce liquid-ordereded and liquid-disordered phase coexistence [121]. To give atomistic resolution interpreation for this phenomena, the atomistic resolution structures and interactions should be correct, which does not seem to the case for Berger/Höltje based model [29] while recent Amber Lipid14 model performs better [101].

Simulation studies have also predicted changes in the acyl chain region which are yet to be experimentally confirmed, e.g. order parameter decrease due to lipid oxidation and changes in order parameter sign in oxidized acyl chain [81].

The usability of MD models for structural interpretation decreases close to the interfacial region since experimental

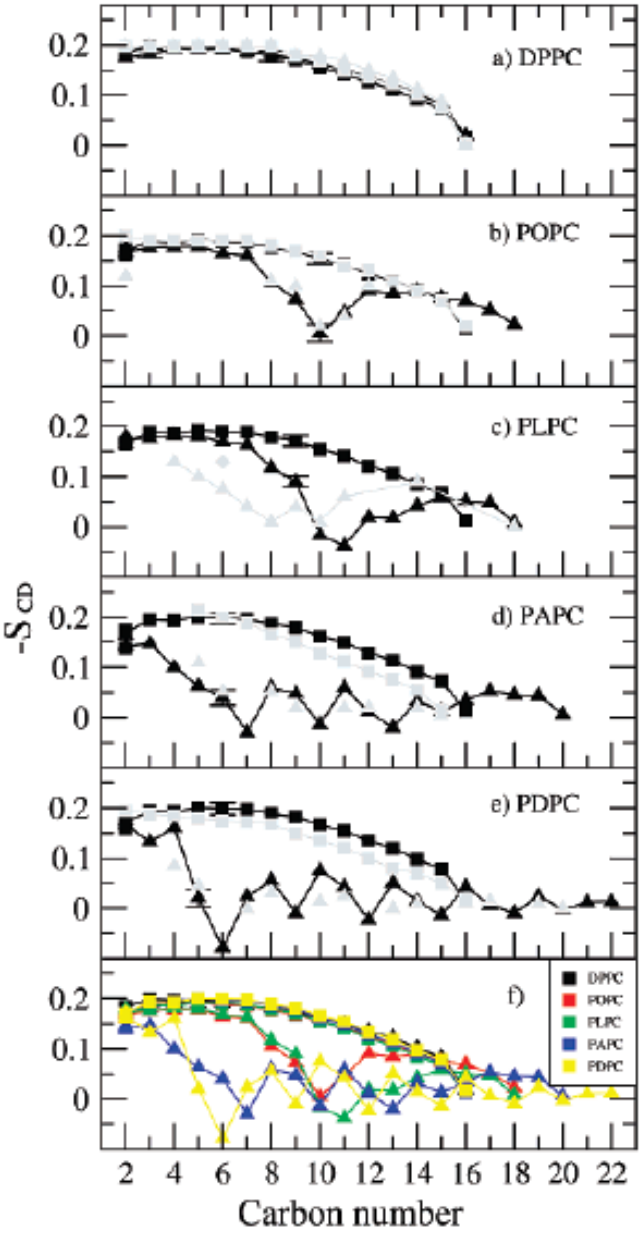

FIG. 6: Figure comparing order parameters in polyunsaturated acyl chains between simulations and experiments adapted from [76]. Order parameters for the sn-1 (squares) and sn-2 (triangles) chains of (A) DPPC, (B) POPC, (C) PLPC, (D) PAPC, and (E) PDPC. Simulation results are shown in full black, and experimental results for comparison in gray. Additionally, part F summarizes the data for all bilayers from the simulations. Experimental order parameters were chosen for comparison as follows. The order parameters for DPPC (T=323K) are based on studies by Petrache et al. [114] whereas the experimental S_{CD} values for PDPC and for the sn-1 chain of POPC (T=310 K) are based on studies by Huber et al. [108] For the sn-1 chain of PDPC, the data set at 310 K is obtained by linearly interpolating between data at 303 and 323 K, whereas for the sn-2 chain the data at 303 K are presented [108]. Experimental values for the sn-2 chain of POPC are based on studies by Seelig et al. [17] A single experimental value is available also for the sn-2 chain of the PLPC bilayer at 313 K (diamond) [19] to compare with our simulated order parameters for PLPC. Together with PLPC, there are also experimental results for PiLPC (T=313K) [19]. Experimental order parameters for the sn-1 and sn-2 chains of PAPC (T=303 K) are based on quadrupole splittings measured by Rajamoorthi et al. [115]. For the sn-1 chain the monotonic decrease through the acyl chain is expected. For the sn-2 chain, values are fitted such that the agreement is as good as possible.

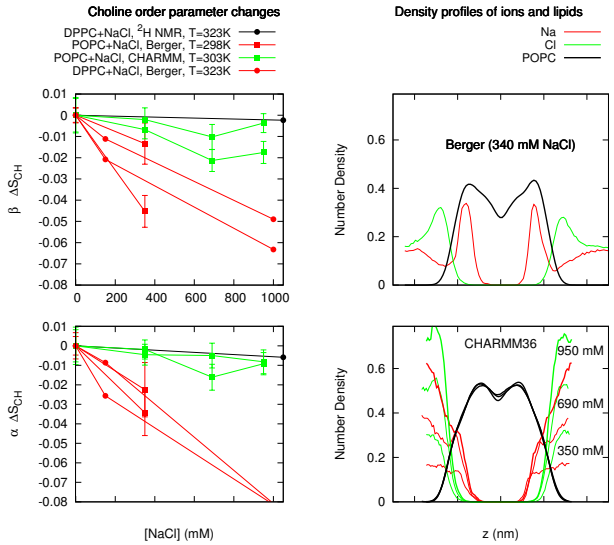

FIG. 7: Changes in choline order parameters (left column) and ion density distributions (right column) as a function of NaCl concentration. Significant order parameter reduction and Na^+ partition is observed with Berger model while only modest order parameter change and ion parition observed with CHARMM36. The results are in line with the electrometer concept connecting the ion partition and choline order parameters changes [36, 59–61]. Consequently, the results show that Na^+ partition is significantly overestimated in the Berger model. For more discussion see [66].

glycerol backbone, choline headgroup and *sn*-2 C_2 segment order parameters are not usually reproduced within experimental error. The forking and low order parameter values for C_2 in the *sn*-2 are related to the parallel orientation of the chain respect to membrane normal [32, 117] which is suggested to have significant contribution e.g. to membrane electrostatic potential [122]. Also the atomistic resolution structures sampled by glycerol backbone and choline headgroup are not yet fully resolved [15, 16, 18, 21, 123, 124]. Unfortunately the accuracy of atomistic resolution models is not yet sufficient to solve these issues. However, the modeling of interfacial region structure has been getting more attention lately [22, 23, 30, 44, 45], thus higher quality models may be expected.

On the other hand, the increase of choline α and β order parameters with dehydration and decrease with cation penetration were correctly reproduced by several models, despite of inaccurate choline structures [30, 66]. The order parameter increase was related to the choline P–N vector tilting more parallel to the membrane normal [30] and order parameter decrease to the cation binding affinity [66]. The observations are in line with previous studies on charge penetration [36, 59–61]. However, choline structural changes due to cholesterol or ion concentration are significantly overestimated in several models [29, 30, 66, 101], especially Na^+ binding affinity [66] (see also Fig. 7). The artificial specific Na^+ binding

induces effectively postively charged membrane which may easily lead to errorneous conclusion due to dominant contribution of electrostatics for various phenomena.

In conclusion, the atomistic resolution MD simulations are invaluable in understanding the structural details and their changes in acyl chain region. However, in applications where lipid interfacial region structure, energetics, electrostatics or ion distributions have significant role, the potential artefacts arising from simulation models must be cafefully taken into account. A typical example of such application would be a study of interactions between charge containing protein in solution and lipid bilayer, simulated in physiological salt concentration [125, 126].

C-H BOND ROTATIONAL DYNAMICS FROM SPIN RELAXATION RATES AND SIMULATIONS

5.This is the first sketch of this section. A lot of references should be added, the text should polished, things should be added and checked and figures should be improved. However, the main strucutre and idea of the section should be visible.

Definition and properties of rotational auto–correlation function

The second order auto-correlation function for the reorientation of the C–H chemical bond axis is defined as

$$g(\tau) = \langle P_2[\vec{\mu}(t) \cdot \vec{\mu}(t+\tau)] \rangle, \tag{4}$$

where P_2 denotes the second Legendre polynomial, $P_2(\xi) = 1/2(3\xi^2 - 1)$, $\vec{\mu}(t)$ is the unitary vector having the direction of the C–H bond at time t, and the angular brackets denote a time-average. For randomly oriented lamellar structures this autocorrelation is connected to the experimentally measurable spin relaxation rates through its Fourier transformation called spectral density [127].

$$j(\omega) = 2 \int_0^\infty \cos(\omega\tau) g(\tau) d\tau. \tag{5}$$

The auto–correlation function for bond orientations always decays to zero in randomly oriented multilamellar samples with long enough time scales due to the diffusion between differently oriented bilayer regions. However, the relaxation processes occur in two distinct timescales and the auto–correlation function can be written as a product of two independent functions [24, 128]

$$g(\tau) = g_{\mathrm{f}}(\tau) g_{\mathrm{s}}(\tau), \tag{6}$$

where $g_{\mathrm{f}}(\tau)$ describes the fast decay (faster than $\sim \mu$s) due to the lipid rotation within bilayer plane and $g_{\mathrm{s}}(\tau)$ describes the slow motions (slower than $\sim \mu$s) from the diffusion between differently oriented bilayer regions. The correlation time of 4.2 ms for the slow decay was estimated from the spin-lattice relaxation rates in rotating frame $R_{1\rho}$ measured with different nutation frequencies for multilamellar POPC sample at 300K [24]. The full auto–correlation decaying to zero, including the contribution from the magic angle spinning (MAS) in kHz region [129], is illustrated in Fig. 8.

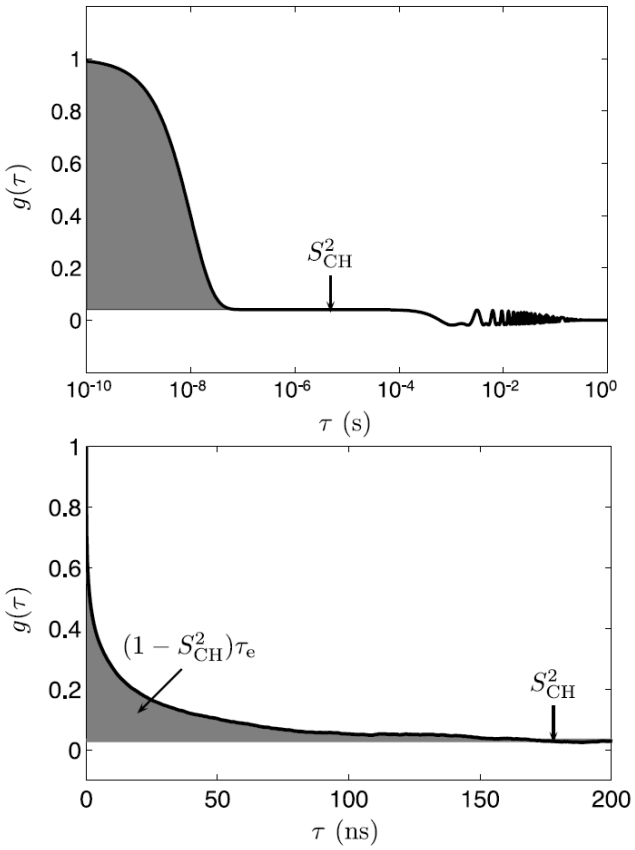

FIG. 8: (Top) Illustration of the auto-correlation function $g(\tau)$ and effective correlation time τ_e for a ^{13}C-H bond in a lipid bilayer in MAS experiment (x–axis with logarithmic scale). Plateau after fast relaxation processes $g(\tau)_f$ is shown between roughly 10^{-7}s and 10^{-4}s. After this timescale the slow relaxation processes $g(\tau)_s$ and oscillation due to MAS [129] are shown. (Bottom) $g(\tau)$ for g_1 segment having the slowest relaxation in POPC bilayer simulated with the Berger based model, illustrating the decay towards S^2_{CH} (x–axis with linear scale). This represents the $g(\tau)_f$ in Eq. 6 and decrease to the plateau in the top figure. The effective correlation time τ_e is equal to the area in gray scaled by $(1 - S^2_{\mathrm{CH}})^{-1}$. Figure adapted from [24].

The $g_{\mathrm{f}}(\tau)$ decays to the plateau having value of S_{ch} within few hundred nanoseconds in liquid crystalline lipid bilayers with planar symmetry [24], as illustrated in Fig 8. The order parameters from ^{2}H NMR and ^{13}C NMR experiments are measured from this plateau [24], thus the rotational correlation function describes the time required to sample conformational space within bilayer plane for single molecule segments. The effective correlation time [127]

$$\tau_e := \int_0^\infty \frac{g_{\mathrm{f}}(\tau) - S^2_{\mathrm{CH}}}{1 - S^2_{\mathrm{CH}}} \mathrm{d}\tau \tag{7}$$

gives intuitively measure for this time; larger τ_e means longer time required for the conformational sampling. With this definition the area between the correlation function and its pleateau becomes $(1 - S^2_{\mathrm{CH}})\tau_e$, as illustrated in Fig. 8.

Detecting C–H bond dynamics experimentally

The C–H bond dynamics in nanosecond timescales can be detected experimentally by measuring the spin relaxation rates R_1^C from ^{13}C NMR and R_1^D from ^{2}H NMR. These are connected the molecular dynamics through the spectral density (Eq. 5) and equations

$$R_1^C = \frac{D^2_{\mathrm{max}} N_{\mathrm{H}}}{20}\left[j(\omega_{\mathrm{H}}-\omega_{\mathrm{C}})+3j(\omega_{\mathrm{C}})+6j(\omega_{\mathrm{C}}+\omega_{\mathrm{H}})\right] \quad (8)$$

and

$$R_1^D = \frac{12\pi^2}{40}\left(\frac{e^2qQ}{h}\right)^2\left[j(\omega_{\mathrm{D}}) + 4j(2\omega_{\mathrm{D}})\right], \quad (9)$$

where ω_{C}, ω_{H} and ω_{D} are the Larmor frequencies for ^{13}C, ^{1}H and ^{2}H, respectively, N_{H} is the number of bound protons, $\frac{D_{\mathrm{max}}}{2\pi}$ ≈22 kHz as in section 2 and $\frac{e^2qQ}{h}$=170kHz as in section 2.

As seen from Eqs. 8 and 9, the numerical values of R_1^C and R_1^D depend on spectral density values at the Larmor frequencies ω_C, ω_H and ω_D. On the other hand, the spectral density value for a given frequency ω depends on the relative amount of relaxation processes with timescales close to ω^{-1}. The Larmor frequencies depend on the spectrometer magnetic field strength and typical timescales for ω^{-1} are between 1-20ns in ^{13}C NMR and ^{2}H NMR experiments. Thus, the R_1^C and R_1^D values measured with standard spectrometer with fixed external field stregth gives a measure of relative amount of relaxation processes with timescales between 1-20ns. Further, the measured changes gives only the change of the relative amount of dynamical processes with these timescales, not the changes in sampling rate. For further discussion and demonstrations see e.g. [24].

For more comprehensive dynamical picture the spin relaxation parameters are measured with different magnetic field strengths by using the field cycling NMR [72, 130–132] and several spectrometers with different magnetic field strengths, as recently reviewed by Leftin and brown [53]. Also the model free approach to measure the effective correlation time (Eq. 7) was recently introduced [24]. The method is based on the combination of experimental order parameter S_{CH}, spin-lattice relaxation rates R_1^C and the transverse magnetization under a spin lock pulse $R_{1\rho}^{\mathrm{plateau}}$ measured with appropriate nutation frequency with equation

$$\tau_{\mathrm{e}} \approx \frac{5R_{1\rho}^{\mathrm{plateau}} - 3.82R_1^C}{D^2_{\mathrm{max}} N_{\mathrm{H}}(1 - S^2_{\mathrm{CH}})}. \quad (10)$$

Analyzing C–H bond dynamics from simulations

Since all the atom coordinates as a function of time are available from molecular dynamics simulations trajectory, the auto–correlation function for each C–H bond can be calculated directly from the definition in Eq. 4. The hydrogen positions can be generated post-simulationally for united atom simulations without explicit hydrogens by creating a trajectory with added hydrogens [24, 76, 133, 134] based on heavy atoms positions and the known hydrocarbon geometries. The ensemble average is taken over all the time intervals and molecules in present in simulation. Since the amount of data decreases for time intervals approaching the simulation total length, only interval lengths less than half of the total simulation length are usually used, for more details see [135].

To calculate the experimentally measurable spin lattice relaxation times from Eqs. 8 and 9, the spectral density must be first calculated from auto-correlation function using Eq. 5. Usually sum of 4 or more exponentials are fitted to the calculated auto–correlation function and then analytical Fourier transform is used to calculate the spectral density [12, 24, 76, 118, 136, 137], however some authors have also used streched exponential exponential functions [133, 134]. The chosen functional form should not affect spin relaxation rate values as long as the fit is good, however the correct form to describe the real relaxation process can be debated [53, 134, 138–140]. Single exponential function is not enought to describe relaxation observed in simulations while 4 gives a reasonable fit [118] which is not surprising since more than one relaxation timescales are expected to be present in bilayer lipids [12, 53, 136, 137]. The R_1^C and R_1^D values are straighforward to calculate from Eqs. 8 and 9 with different Larmor frequencies or as a function of external field by using the fitted spectral density function.

The effective correlation time τ_e can be calculated directly from the integrated area below the correlation function, see Fig. 8 or by using the exponential sum fitted to the correlation function and Eq. 30 in Ref. [24]. The $R_{1\rho}$, used to determine effective correlation time experimentally in Eq. 7, cannot be calculated from simulations directly since its value may depend also on the slow relaxation dynamics ($g_s(t)$ in Eq. 6) which is not present in simulations [24]. The same applies to the calculation of NOESY relaxations rates and in this case decay time of 170 ns was assumed for the $g_s(t)$ [141], while 4.2 ms was measured by Ferreira et al. [24].

Comparing C–H bond dynamics between simulations and NMR experiments

Spin relaxation rates R_1^C and R_1^D with one [24, 76, 92, 109, 118] or more [12, 92, 112, 133, 134, 137, 139] external magnetic field strengths have been compared between experiments and simulations mainly for CHARMM (Fig. 9) and Berger based models (Fig. 10). The comparison with several magnetic field strengths shows good agreement between ex-

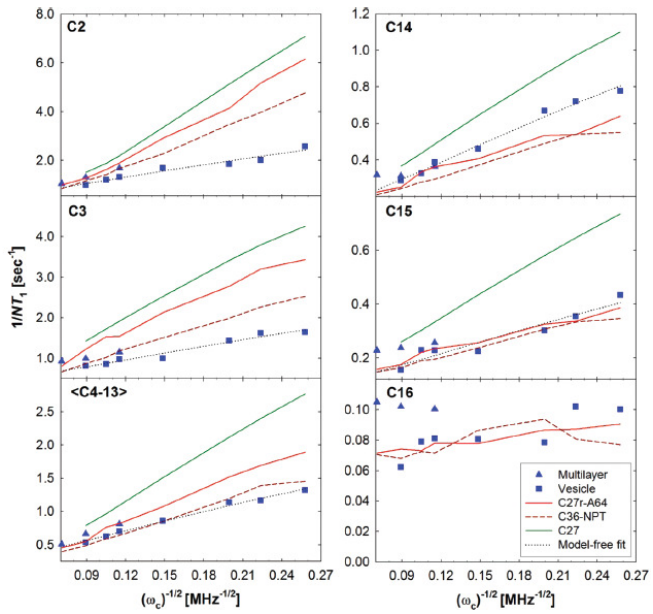

FIG. 9: Comparison of R_1^C dependence on magnetic field between experiments [139, 142] and different CHARMM simulations [44] for acyl chain carbons (DPPC bilayer in 323K) adapted from [44]. Experiments as points; MD simulations as solid and dashed lines; and a model-free fit to the vesicle data as dotted lines.

periments with large larmor frequencies for both CHARMM and Berger based models in Figs. 9 and 10 A), respectively. With increasing larmor frequencies both models show a good agreement deep in the acyl chain region while closer to the interfacial motional modes corresponding lower Larmor frequencies seems to over presented in both models. Since lower larger Larmor frequencies correspond larger correlation times, this may indicate too slow dynamics closer to the interfacial region.

This is in line with the comparison between experimental and simulated effective correltion time for Berger based POPC model, shown in Fig. 10 C); the effective correlation times for acyl chain region agrees with experiments while closer to the interfacial region the correlation times are too large in simulations. The discrepancies for R_1^C between experiments and simulations for acyl chain region seen in Fig. 10 B) indicate, however, that different dynamical processes are not correctly balanced in simulations despite of good agreement for τ_e. On the other hand, good agreement for spin lattice relaxation rates for polyunsaturated acyl chains between experiments with large Larmor frequneciens and simulations with both, CHARMM [112, 118] and Berger based [76] models, are reported.

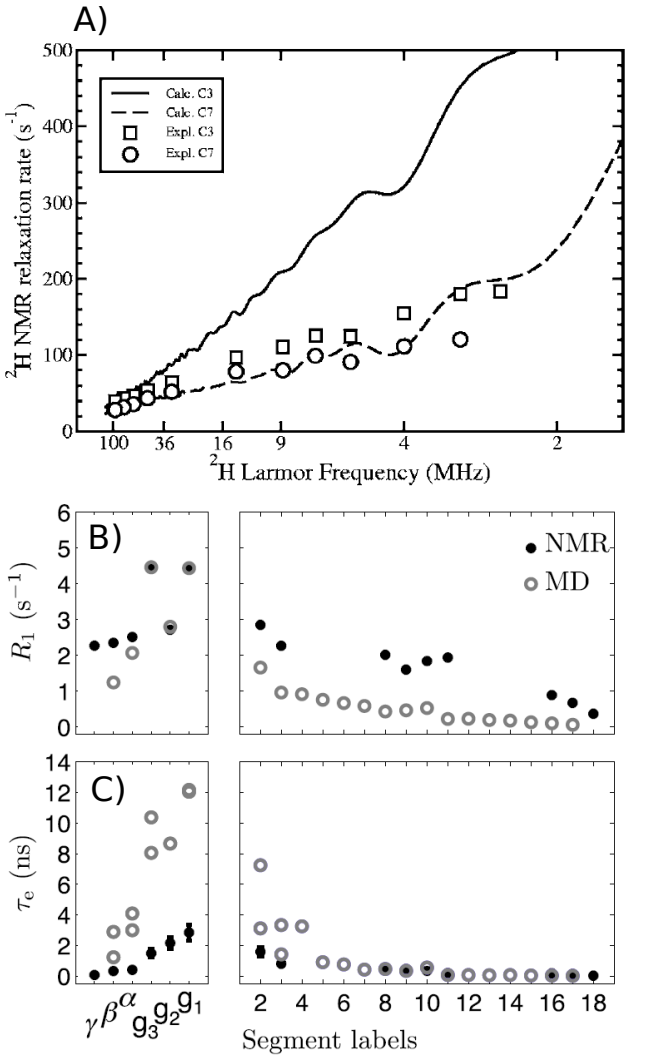

FIG. 10: Comparisons between Berger based models and experimental spin relaxation rates: A) R_1^D dependence on magnetic field for acyl chain carbons (DMPC bilayer at 300K) adapted from [134], B) R_1^C measured with field strength correspondin to the Larmor frequency of 125 MHz for ^{13}C (POPC bilayer at 298K) and C) effective correlation times τ_e (POPC bilayer at 298K) adapted from Ferreira et al. [24].

Interplay between simulations and NMR spin lattice relaxation times: Validation and interpretation of dynamics

By measuring single spin relaxation times it is almost impossible to draw any conclusions about molecular dynamics due to their complicated connection through the spectral density. Even changes of relaxation times cannot be directly related to molecular dynamics without further information, since, e.g. faster dynamics may lead to the decrease or increase of spin relaxation times, depending (i) on the other dynamics processes present and (ii) the used magnetic field strength as demonstrated, for example in [24].

Careful studies of spin relaxation times as a function of temperature and magnetic field to overcome this issue were recently reviewed by Leftin and Brown [53]. From compilation of different experimental data sets it was possible to conclude, for example, that the interfacial region of lipid molecules has slower dynamics than the acyl chains [53]. Another successfull approach to interpret the spin relaxation times has been to use the atomistic resolution of molecular dynamics simulations to reproduce first the measured changes and then to analyze the dynamical changes from the simulation trajectory [109, 118, 143]. This has been especially useful in the studies of polyunsaturated acyl chain dynamics which concluded – by combining the simulation and NMR relaxation data – that the double bonds speed us the chain dynamics due to flexible dihedrals next to the double bonds [109, 118–120].

To ease the interpretation of the measured spin relaxation times Ferreira et al. recently introduced a model-free connection between effective correlation time and directly measurable spin relaxation rates [24]. The main advantages of the effective correlation time is that its connection to molecular dynamics is straightforward in the sense that the general dynamics are faster when effective correlation times decrease and *vice versa* and that it can be quantitatively compared to simulations. As shown in Fig. 10 these experiments immediately show that the glycerol backbone has the slowest dynamics of lipid segments (in agreement with conclusions from the combination of several previous experimental sets [53]) and that the dynamics of these is significantly underestimated by the Berger model.

Most importantly, the rough agreement of spin relaxation rates and effective correlation times between simulations and experiments shows that the rotational dynamical processes present in simulations has the correct order of magnitude [12, 24, 76, 92, 92, 109, 112, 118, 133, 134, 137, 139]. Consequently, the dynamical visualizations of simulation trajectories (videos) can be considered as realistic intuitive presentations of lipid bilayers. However, in more detailed studies it should be kept in mind that all the dynamical (and also structural) details are strictly speaking not correct.

Lipid rotational dynamics have been often interpreted by using the so called wobble in the cone model [12, 72, 137, 139, 140]. The main idea of the model is that the whole lipid molecule is wobbling as a cone such that all segments share the time scale for this motion. In addition, each segments has further timescales related to their dynamincs inside the cone. The auto–correlation functions assuming the wobble in the cone model can be nicely fit to the simulation data and also some experimental results can be reproduced. However, also auto–correlation functions having different type of dynamics can be used to do the same. On the other hand, it has been recently pointed out that significant changes of structure and dynamics experienced in acyl chain region may not hinge on the headgroup [30, 144] indicating weak coupling between these segments. This idea is also in line with one possible interpretation given in recent field cycling experiments [132]. In addition, the role of membrane undulations in the relaxation data measured with low frequencies is under discussion [53, 138–140].

In conclusion, the overall timescale of rotational dynamics is correct in simulations while the exact correlation times and relaxation processes are not fully reproduced. More experimental and simulation studies are needed to fully understand current quality of dynamics in current models. To interpretate the relaxation prcosesses present in lipid bilayer, a model which can be shown to agree with experiments on all fast timescales is needed.

STUCTURE FACTORS FROM SCATTERING AND SIMULATIONS

Form factor measured with X-ray or Neutron scattering

Small-angle X-ray or neutron scattering (SAXS/SANS)) experiments can be used to probe the overall structure of the lipid bilayer, in particular scattering length density profiles along normal axis. The measured scattering intensity can be written as $I(q) \sim |F(q)|^2 S(q)/C_{\mathrm{LF}}$, where $F(q)$ is the bilayer form factor, $S(q)$ is the structure factor and C_{LF} the Lorentz correction ($C_{\mathrm{LF}} = q^2$ for free-floating lipid vesicles and $C_{\mathrm{LF}} = q$ for aligned bilayers). The structure factor characterizes the crystalline or quasicrystalline structure of bilayer stacks and the form factor describes the scattering length density distribution of the lipid bilayer itself along the bilayer normal.

Here we are mainly interested in the form factor since the focus on lipid bilayer structure. The scattering intensity can be measured with SAXS or SANS from unilamellar vesicles (ULVs), oriented multilamellar bilayes (ORI) and un-oriented multilamellar vesicles (MLVs). Information about the structure factor is needed to extract the form factor from the scattering intensity, except for positionally uncorrelated ULVs, where $S(q) = 1$ [10]. For multibilayers in the fluid phase the structure factor is given by the Caillé theory [145, 146]. For oriented samples the form factor is determined by scaling a 2D fit of the Caillé structure factor (for in-plane and out-of-plane scattering constributions) to the measured scattering intensity [146, 147]. For MLVs the form factor needs to be modeled in combination with the structure factor to fit the scattering intensity [148]. This is achieved by using a specific real-space description of the bilayer structure (scattering length density profile). Note that different real-space model yield equivalent form factors. Thus, the form factors are not highly sensitive to the applied model. Different technical issues must be carefully considered in all scattering experiments, in particular subtracting background scattering and, in the case of ORI and MLVs, fitting accuracy. The form factors measured from different geometries [147, 149] and research groups are in good agreement as demonstrated in Fig. 11, indicating that the bilayer structure is similar in different preparations of the same lipid and that the technique is highly robust.

By following the notation from Ref. [25], the form factor

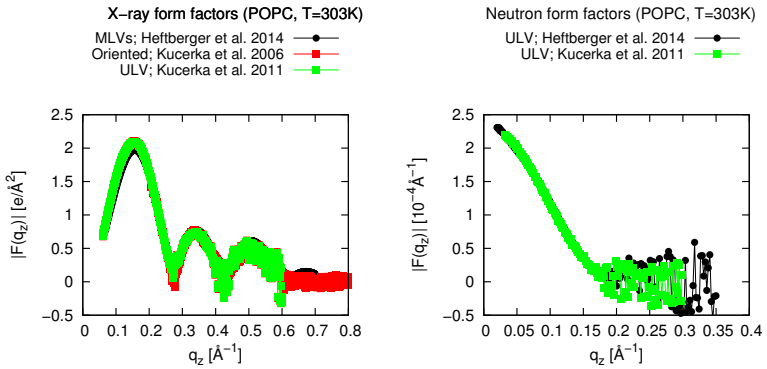

FIG. 11: Comparison of reported X-ray (Panel A) and neutron (Panel B) form factors for POPC bilayers at 303K in different geometries measured in different groups.

is connected to the bilayer atom number density through the equation

$$|F(q)| = |\int_{-D/2}^{D/2} (\sum_{\alpha} f_\alpha(q_z) n_\alpha(z) - \rho_s) \exp(izq_z) \mathrm{d}z|, \tag{11}$$

where $n_\alpha(z)$ in the atom α number density as a function of membrane normal coordinate z, $f_\alpha(q_z)$ is the atom scattering length density, ρ_s is the solvent scattering length density and integral spans over the bilayer of thickness D. The atom scattering length density $f_\alpha(q_z)$ depends on the type of scattering used since X-ray photons interact with the sample's electron cloud, while neutron scatter off nuclei in a particular manner. This leads also to distinct contrast for different parts of the membrane. X-rays, for example are most sensitive to the electron-rich phospholipid headgroups. Neutron experiments typically explore the contrast between hydrogen and deuterium [10], e.g. SANS on protiated lipid bilayers suspended in 100% D_2O probes mainly the membrane's hydrophobic thickness. Consequently, highest-structural resolution can be achieved upon combining SAXS and SANS experiments [147, 150].

For symmetric lipid bilayers Eq. 11 simplifies to the widely used form

$$|F(q)| = |\int_{-D/2}^{D/2} \Delta\rho_e(z) \cos(zq_z) \mathrm{d}z|, \tag{12}$$

where $\Delta\rho_e(z)$ is the scattering length density difference between solvent and bilayer.

6.Discussion about related issues can be found at: https://github.com/NMRLipids/NMRLipids_V-Review/issues/1

7.The discussion is going in at: https://github.com/NMRLipids/NMRLipids_V-Review/issues/2

Form factor calculation from simulations

The atomic number densities $n_\alpha(z)$ are straighforward to calculcate from simulations and then substitute into Eq. 11 to calculate the form factor. The atomic scattering length densities $f_\alpha(q_z)$ for neutrons are available in the literature [151]. For x-ray scattering pointwise valence electron location at atom positions is usually assumed and in this case the $f_\alpha(q_z)$ becomes the number of electron per atom, while gaussian electron distribution around atom positions [152] or an analytical expression $f_\alpha(q_z) = \sum_{j=1}^{4} a_j e^{-b_j(q/4\pi)^2} + c$ with parameters a_j, b_j and c taken from [153] are assumed in some studies [152], including the widely used SIMtoEXP software [25]. The effect of these choises to the electron density profiles was discussed by Benz et al. [152], however, it is not clear how stronhly this would affect form factors calculated from simulations. In most simulations the bilayer is symmetric, thus the simpler Eq. 12 is used.

The small bilayer patches used in simulations might depress bilayer undulation modes which are present in large scale experiments [154]. Braun et al. showed that undulations seen in large enough simulations do not change the position of form factor minimas but depress the peak hights in the lobes [154]. Since the undulations are expected to be present in the experiments, the potential discrepancies between simulations and experiments in the lobe heights may be explained by the lack of undulation motions in simulations. The undulation effects are also sometimes reduced from the experimentally reported form factors by scaling q in x–axis, however, the scaling factor is very close to 1 [147].

Simulations give the form factors on absolute scale while experiments obtain them only on a relative scale, thus the experimental form factors from different sources has to be scaled for comparison [25, 150]. For example, in SIMtoEXP program the scaling is performed using the scaling factor k determined from equation

$$k = \frac{\sum_{i=1}^{N} \frac{|F_s(q_i)||F_e(q_i)|}{(\Delta F_e(q_i))^2}}{\sum_{i=1}^{N} \frac{|F_e(q_i)|^2}{(\Delta F_e(q_i))^2}}, \tag{13}$$

where $F_e(q)$ and $F_s(q)$ are experimental and simulated form factors, respectively, $\Delta F_e(q)$ is the uncertainty of the exper-

imental form factor and the summation goes over all N data points [25, 150].

8.More discussion at:

https://github.com/NMRLipids/NMRLipids_V-Review/issues/3

and

https://github.com/NMRLipids/NMRLipids_V-Review/issues/4

Comparing form factors between simulations and experiments

The comparison to experimental area per molecule values to validate the lipid density in simulations [77] has been often replaced nowdays with more direct comparison [5] using x-ray form factors [22, 39, 43–50, 99–101, 112, 113]. In some studies the comparison is complemented with the comparison to the neutron scattering data [45, 46, 48–50, 101] In general the models produce form factors in good agreement with experiments, especially at small q values indicating that the overall bilayer dimensions, like thickness, are reproduced reasonably well. However, the agreement gets often worse toward higher q values [22, 43–47, 49, 50, 99–101, 112, 113] indicating discrepancies in fine structural details such as, e.g. hydrocarbon chain packing or headgroup structure(see e.g. Fig. 12). Typically, the comparison of experimental and simulated form factors is based on visual inspection while also quantitative measure for simulated form factor quality has been suggested [25]. In studies also Fourier transform coeffiecients are compared [152]

Also changes in form factor due to temperature [46, 102], cholesterol concentration [100, 101] and acyl chain polyunsaturation [112, 118] have been compared between simulations and experiments [9, 118, 147, 155–159]. Simulation generally reproduce the decreased thickness and increased area with increasing temperature [46, 102] and polyunsaturation level [112, 118], as well as increased thickness and decreased area with increasing cholesterol concentration [100, 101]. However, the temperature dependence is underestimated for some systems [46, 102] while cholesterol effect is overestimated [100, 101]. Example of such comparison is shown in Fig. 12.

In conclusion, all the state of the art simulation models gives form factors close to experimental data in various conditions indicating reasonable agreement for average bilayer dimensions. Also the qualitative changes are reproduced, however, discrepancies prevail for quantitative details of bilayer structure and changes with temperature and admixture of other lipids such as cholesterol.

9.The more detailed discussion can be found at:

https://github.com/NMRLipids/NMRLipids_V-Review/issues/5

Interplay between simulations and scattering experiments: Validation and interpretation

Similarly to NMR order parameters, the form factor gives accurate information about lipid bilayer structure but the structure cannot be uniquely resolved from the experimental data only. To give structural intepretation of order parameters, the model for sampled conformations of single molecules are needed while to interpret the scattering form factor data the model for the atom number densities, $n_\alpha(z)$ in Eq. 11, is needed. Several models developed and used for this purpose are reviewed by Heberle et al. [160].

Similarly to the NMR order parameters, also MD simulations can be used in the structural interpretation if they reproduce the experimental form factors. And in turn, if simulation model do not reproduce the experimental form factor its structure is not realistic. The comparison between experimental and simulated form factors has been done in several studies for both purposes, to validate the simulations model [22, 39, 43–50, 99–101, 112, 113] and to intepret the experiments [150, 161–164]. The simulations have been also used to improve the fitting based structural models [**?**].

In studies where the main goal is to interpret the form factors using MD simulations instead of validating the model, the area per molecule is often fixed to a certain value in order to reproduce the experimental form factor better [150, 161–164]. With this constraint it is indeed possible to get the form factors close to the experiments, however, careful comparisons between experimental form factors, MD simulations and SDP model suggest small but measurable structural differences [150, 164]. The form factor from the SDP model is in better agreement with simulations and the extracted stuctural parameters indicate differences especially in the headgroup region [150, 164] which is in agreement with the comparions between simulations and NMR order parameter indicating issues in the same region [30], see also section **??**.

CONCLUSIONS

Recent studies quantitatively comparing atomistic resolution structure and dynamics of lipid bilayer between experiments using C–H bond order parameters, spin relaxation rates and scattering form factors are reviewed. The purpose of these studies is to quantify the atomistic resolution structural and dynamical quality of simulation models as well as to give an atomistic resolution interpretation for the experimental results. For interpretation of these experiments the atomistic resolution MD simulations reproducing all the experiments would be an ultimate tool since the same model can be used to jointly interpret NMR and scattering data. For the same reason, this atomistic resolution model would be most likely a realistic representation for atomistic resolution strucutre and dynamics of lipid bilayers. The main conclusion of this review is that the current MD simulations are not quite yet on the level to perform this task, however, in several aspects indicate that there is potential to improve the models to become truly realistic atomistic resolution representations of these systems.

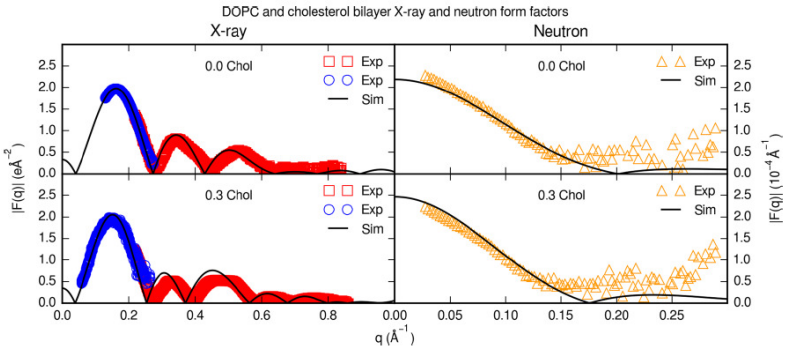

FIG. 12: Example of comparison between simulation model and experiment. The agreement is better with low q values and cholesterol induced thickening is overestimated. Figure adapted from Madej et al. [101].

More specific conclusions are the following:
- The order parameters for each C–H bond in lipid molecules in bilayers can be measured with high quantitative accuracy with both 2H NMR and 13C NMR and this data is available for wide range of lipids in different conditions. Comparison of this data to simulations gives a very detailed picture about the quality of sampled atomistic resolution structures in lipid bilayer and may also help in structural interpretation of experiments. The order parameter changes with varying conditions can be used to study and compare structural changes between simulations and experiments.
- The main conclusions from the comparison of order parameters between experiments and simulations are: 1) the acyl chain structures are generally described realistically for PC lipid bilayers in simulations, 2) the changes in acyl chain region are qualitatively correct but not always quantitatively, 3) the glycerol backbone and choline structures are not within experimental error for any available model and 4) the results depending on structure and energetics of these sections, like ion binding and lipid–cholesterol interactions should be taken with caution.
- The C–H bond rotational dynamics has correct timescale in simulations models for which comparison has been done. Most likely the same applies for all models. However, more careful comparison reveals that, e.g. the glycerol backbone dynamics is too slow in Berger model. Also for CHARMM model all relaxation prosess do not seem to correctly described.
- The development in the scattering methodology has allowed the direct comparison of whole bilayer structure between experimental form factor and simulations. This is complementary to the NMR order parameter which are related to the sampled structures of individual molecules. These comparisons show that the structural lipid bilayer properties like thickness and area per molecule are close to real values, however, it seems that there is room for improvement especially in the lipid headgroup region, in agreement with conclusions from NMR experiments. Additionally, wide-angle x-ray scattering of lipid bilayers, probing short-range positional correlations between hydrocarbons should serve in the future as an additional guide of MD simulations and yield in turn important insight on structural properties of the bilayers (see e.g. [**?**]).

When applying lipid bilayer simulations to study complicated biochemical systems it is crucial to recognize potential artefacts arising from the inaccuracies revealed by these comparisons. Hyphotetical example of a situation where artificial conclusions might be difficult to avoid would be study of protein approaching PC lipid bilayer in physiological NaCl concentration. If the above mentioned issues are not carefully taken into account one might choose a model where the protein is approaching an effectively positively charged lipid bilayer due to artificial Na+ binding with incorrect choline structure. In addition to this the protein might be incorrectly folded already in the bulk water [**?**].

* samuli.ollila@aalto.fi

[1] J. N. Israelachvili, S. Marcelja, and R. G. Horn, Q. Rev. Biophys. **13**, 121 (1980).
[2] R. E. Jacobs and E. Oldfield, Prog. Nucl. Mag. Res. Sp. **14**, 113 (1981).
[3] J. H. Davis, Biochim. Biophys. Acta **737**, 117 (1983).
[4] M. Bloom, E. Evans, and O. G. Mouritsen, Quarterly Reviews of Biophysics **24**, 293 (1991), ISSN 1469-8994, URL http://journals.cambridge.org/article_S0033583500003735.
[5] J. F. Nagle and S. Tristram-Nagle, Biochem. Biophys. Acta **1469**, 159 (2000).
[6] A. G. Lee, Biochim. Biophys. Acta **1666**, 62 (2004).
[7] P. K. J. Kinnunen, The Open Biology Journal **2**, 163 (2009).
[8] G. Pabst, N. Kucerka, M.-P. Nieh, M. Rheinstdter, and J. Katsaras, Chem Phys Lipids **163**, 460 (2010), ISSN 0009-3084, URL http://www.sciencedirect.com/science/article/B6T2N-4YRHCWP-1/2/539e61bf10683661bd62b21d109fcb9a.
[9] N. Kučerka, M. P. Nieh, and J. Katsaras, Biochim Biophys Acta **1808**, 2761 (2011), ISSN 0006-3002.
[10] D. Marquardt, F. A. Heberle, J. D. Nickels, G. Pabst, and J. Katsaras, Soft Matter (2015).

[11] P. van der Ploeg and H. J. C. Berendsen, The Journal of Chemical Physics **76** (1982).

[12] R. W. Pastor, R. M. Venable, M. Karplus, and A. Szabo, The Journal of Chemical Physics **89** (1988).

[13] A. Abragam, *The Principles of Nuclear Magnetism* (Oxford University Press, 1961).

[14] A. Seelig and J. Seelig, Biochemistry **13**, 4839 (1974).

[15] H. U. Gally, W. Niederberger, and J. Seelig, Biochemistry **14**, 3647 (1975).

[16] A. Seelig and J. Seelig, Biochemistry **16**, 45 (1977).

[17] J. Seelig and N. Waespe-Sarcevic, Biochemistry **17**, 3310 (1978).

[18] L. Strenk, P. Westerman, and J. Doane, Biophys. J. **48**, 765 (1985).

[19] J. E. Baenziger, H. C. Jarrel, R. J. Hill, and I. C. P. Smith, Biochemistry **30**, 894 (1991).

[20] M. Hong, K. Schmidt-Rohr, and D. Nanz, Biophys. J. **69**, 1939 (1995).

[21] K. S. Bruzik and J. S. Harwood, Journal of the American Chemical Society **119**, 6629 (1997).

[22] J. Chowdhary, E. Harder, P. E. M. Lopes, L. Huang, A. D. MacKerell, and B. Roux, J. Phys. Chem. B **117**, 9142 (2013).

[23] P. Prakash and R. Sankararamakrishnan, J. Comp. Chem. **31**, 266 (2010).

[24] T. M. Ferreira, O. H. S. Ollila, R. Pigliapochi, A. P. Dabkowska, and D. Topgaard, J. Chem. Phys. **142**, 044905 (2015), URL http://scitation.aip.org/content/aip/journal/jcp/142/4/10.1063/1.4906274.

[25] N. Kuerka, J. Katsaras, and J. Nagle, Journal of Membrane Biology **235**, 43 (2010), ISSN 0022-2631.

[26] J. Seelig, Q. Rev. Biophys. **10**, 353 (1977).

[27] J. D. Gross, D. E. Warschawski, and R. G. Griffin, J. Am. Chem. Soc. **119**, 796 (1997).

[28] S. V. Dvinskikh, V. Castro, and D. Sandstrom, Phys. Chem. Chem. Phys. **7**, 607 (2005).

[29] T. M. Ferreira, F. Coreta-Gomes, O. H. S. Ollila, M. J. Moreno, W. L. C. Vaz, and D. Topgaard, Phys. Chem. Chem. Phys. **15**, 1976 (2013).

[30] A. Botan, F. Fernando, J. F. Patrick Franois, M. Javanainen, M. Kanduc, W. Kulig, A. Lamberg, C. Loison, A. P. Lyubartsev, M. S. Miettinen, et al., The Journal of Physical Chemistry B **0**, null (0), pMID: 26509669, http://dx.doi.org/10.1021/acs.jpcb.5b04878, URL http://dx.doi.org/10.1021/acs.jpcb.5b04878.

[31] M. Hong, K. Schmidt-Rohr, and A. Pines, J. Am. Chem. Soc. **117**, 3310 (1995).

[32] A. Seelig and J. Seelig, Biochimica et Biophysica Acta (BBA) - Biomembranes **406**, 1 (1975).

[33] H. U. Gally, G. Pluschke, P. Overath, and J. Seelig, Biochemistry **20**, 1826 (1981).

[34] A. K. Engel and D. Cowburn, FEBS Letters **126**, 169 (1981).

[35] B. Perly, I. C. P. Smith, and H. C. Jarrell, Biochemistry **24**, 1055 (1985).

[36] H. Akutsu and J. Seelig, Biochemistry **20**, 7366 (1981).

[37] B. Bechinger and J. Seelig, Chem. Phys. Lipids **58**, 1 (1991).

[38] O. Berger, O. Edholm, and F. Jähnig, Biophys. J. **72**, 2002 (1997).

[39] C.-J. Högberg, A. M. Nikitin, and A. P. Lyubartsev, J. Comput. Chem. **29**, 2359 (2008).

[40] D. Poger, W. F. Van Gunsteren, and A. E. Mark, J. Comput. Chem. **31**, 1117 (2010).

[41] J. P. Ulmschneider and M. B. Ulmschneider, J. Chem. Theory Comput. **5**, 1803 (2009).

[42] A. Kukol, J. Chem. Theory Comput. **5**, 615 (2009).

[43] S.-W. Chiu, S. A. Pandit, H. L. Scott, and E. Jakobsson, J. Phys. Chem. B **113**, 2748 (2009).

[44] J. B. Klauda, R. M. Venable, J. A. Freites, J. W. O'Connor, D. J. Tobias, C. Mondragon-Ramirez, I. Vorobyov, A. D. M. Jr, and R. W. Pastor, J. Phys. Chem. B **114**, 7830 (2010).

[45] C. J. Dickson, L. Rosso, R. M. Betz, R. C. Walker, and I. R. Gould, Soft Matter **8**, 9617 (2012).

[46] J. P. M. Jämbeck and A. P. Lyubartsev, J. Phys. Chem. B **116**, 3164 (2012).

[47] A. Maciejewski, M. Pasenkiewicz-Gierula, O. Cramariuc, I. Vattulainen, and T. Rog, J. Phys. Chem. B **118**, 4571 (2014).

[48] R. Tjörnhammar and O. Edholm, J. Chem. Theory Comput. **10**, 5706 (2014).

[49] C. J. Dickson, B. D. Madej, . A. Skjevik, R. M. Betz, K. Teigen, I. R. Gould, and R. C. Walker, J. Chem. Theory Comput. **10**, 865 (2014).

[50] S. Lee, A. Tran, M. Allsopp, J. B. Lim, J. Henin, and J. B. Klauda, J. Phys. Chem. B **118**, 547 (2014).

[51] V. Castro, S. V. Dvinskikh, G. Widmalm, D. Sandstrm, and A. Maliniak, Biochimica et Biophysica Acta (BBA) - Biomembranes **1768**, 2432 (2007).

[52] V. Castro, B. Stevensson, S. V. Dvinskikh, C.-J. Högberg, A. P. Lyubartsev, H. Zimmermann, D. Sandström, and A. Maliniak, Biochim. Biophys. Acta - Biomembranes **1778**, 2604 (2008).

[53] A. Leftin and M. F. Brown, Biochim. Biophys. Acta - Biomembranes **1808**, 818 (2011).

[54] D. Marsh, *Handbook of Lipid Bilayers, Second Edition* (RSC press, 2013).

[55] Journal of Molecular Biology **425**, 2973 (2013).

[56] A. Leftin, T. Molugu, C. Job, K. Beyer, and M. Brown, Biophysical Journal **107**, 2274 (2014).

[57] A. Ulrich and A. Watts, Biophys. J. **66**, 1441 (1994).

[58] K. Mallikarjunaiah, A. Leftin, J. J. Kinnun, M. J. Justice, A. L. Rogozea, H. I. Petrache, and M. F. Brown, Biophysical Journal **100**, 98 (2011), ISSN 0006-3495, URL http://www.sciencedirect.com/science/article/pii/S0006349510013792.

[59] C. Altenbach and J. Seelig, Biochemistry **23**, 3913 (1984).

[60] J. Seelig, P. M. MacDonald, and P. G. Scherer, Biochemistry **26**, 7535 (1987).

[61] P. G. Scherer and J. Seelig, Biochemistry **28**, 7720 (1989).

[62] M. F. Brown and J. Seelig, Biochemistry **17**, 381 (1978).

[63] J. Douliez, A. Lonard, and E. Dufourc, Biophysical Journal **68**, 1727 (1995), ISSN 0006-3495, URL http://www.sciencedirect.com/science/article/pii/S0006349595803504.

[64] E. Kuchinka and J. Seelig, Biochemistry **28**, 4216 (1989).

[65] M. Roux and M. Bloom, Biochemistry **29**, 7077 (1990).

[66] A. Catte, M. Girych, M. Javanainen, M. S. Miettinen, L. Monticelli, J. Määttä, V. S. Oganesyan, and O. H. S. Ollila, *The electrometer concept and binding of cations to phospholipid bilayers* (2015), dOI: 10.5281/zenodo.32175.

[67] F. Aussenac, M. Laguerre, J.-M. Schmitter, and E. J. Dufourc, Langmuir **19**, 10468 (2003).

[68] G. Raffard, S. Steinbruckner, A. Arnold, J. H. Davis, and E. J. Dufourc, Langmuir **16**, 7655 (2000).

[69] C. R. Sanders and J. P. Schwonek, Biochemistry **31**, 8898 (1992).

[70] L. E. Marbella, B. Yin, and M. M. Spence, The Journal of Physical Chemistry B **119**, 4194 (2015).

[71] J. Becker, A. Comotti, R. Simonutti, P. Sozzani, and K. Saalwchter, The Journal of Physical Chemistry B **109**, 23285 (2005).

[72] V. N. Sivanandam, J. Cai, A. G. Redfield, and M. F. Roberts, Journal of the American Chemical Society **131**, 3420 (2009).

[73] S. V. Dvinskikh, V. Castro, and D. Sandstrom, Phys. Chem. Chem. Phys. **7**, 3255 (2005).

[74] C.-J. Hgberg, , and A. P. Lyubartsev*, The Journal of Physical Chemistry B **110**, 14326 (2006).

[75] *The nmrlipids project, on the signs of the order parameters* (2014), URL http://web.archive.org/web/20150414085027/http://nmrlipids.blogspot.fi/2014/04/on-signs-of-order-parameters.html.

[76] S. Ollila, M. T. Hyvönen, and I. Vattulainen, J. Phys. Chem. B **111**, 3139 (2007).

[77] D. P. Tieleman, S. J. Marrink, and H. J. C. Berendsen, Biochim. Biophys. Acta **1331**, 235 (1997).

[78] L. Vermeer, B. de Groot, V. Rat, A. Milon, and J. Czaplicki, Eur. Biophys. J. **36**, 919 (2007), ISSN 0175-7571, URL http://dx.doi.org/10.1007/s00249-007-0192-9.

[79] D. Poger and A. E. Mark, J. Chem. Theory Comput. **8**, 4807 (2012).

[80] M. Bachar, P. Brunelle, D. P. Tieleman, and A. Rauk, J. Phys. Chem. B **108**, 7170 (2004).

[81] J. Wong-ekkabut, Z. Xu, W. Triampo, I.-M. Tang, D. P. Tieleman, and L. Monticelli, Biophysical Journal **93**, 4225 (2007), ISSN 0006-3495, URL http://www.sciencedirect.com/science/article/pii/S0006349507716752.

[82] A. Vogel and S. Feller, The Journal of Membrane Biology **245**, 23 (2012), ISSN 0022-2631.

[83] E. Egberts and H. J. C. Berendsen, J. Chem. Phys. **89**, 3718 (1988).

[84] T. R. Stouch, Molecular Simulation **10**, 335 (1993).

[85] E. Egberts, S.-J. Marrink, and H. Berendsen, European Biophysics Journal **22**, 423 (1994), ISSN 0175-7571, URL http://dx.doi.org/10.1007/BF00180163.

[86] J. W. Essex, M. M. Hann, and W. G. Richards, Philos. T. Roy. Soc. B **344**, 239 (1994).

[87] A. Robinson, W. Richards, P. Thomas, and M. Hann, Biophys. J. **67**, 2345 (1994).

[88] M. T. Hyvönen, M. Ala-Korpela, J. Vaara, T. T. Rantala, and J. Jokisaari, Chem. Phys. Lett. **246**, 300 (1995).

[89] V. Kothekar, Ind. J. Biochem. Biophys. **33**, 431 (1996).

[90] D. P. Tieleman and H. J. C. Berendsen, J. Chem. Phys. **105**, 4871 (1996).

[91] W. Shinoda, N. Namiki, and S. Okazaki, J. Chem. Phys. **106**, 5731 (1997).

[92] J. B. Klauda, R. M. Venable, A. D. M. Jr., and R. W. Pastor, in *Computational Modeling of Membrane Bilayers*, edited by S. E. Feller (Academic Press, 2008), vol. 60 of *Current Topics in Membranes*, pp. 1 – 48.

[93] S. W. I. Siu, R. Vcha, P. Jungwirth, and R. A. Bckmann, The Journal of Chemical Physics **128** (2008).

[94] E. J. Dufourc, E. J. Parish, S. Chitrakorn, and I. C. P. Smith, Biochemistry **23**, 6062 (1984).

[95] M. Lafleur, P. Cullis, and M. Bloom, European Biophysics Journal **19**, 55 (1990), ISSN 0175-7571, URL http://dx.doi.org/10.1007/BF00185086.

[96] J. A. Urbina, S. Pekerar, H. biao Le, J. Patterson, B. Montez, and E. Oldfield, Biochimica et Biophysica Acta (BBA) - Biomembranes **1238**, 163 (1995), ISSN 0005-2736, URL http://www.sciencedirect.com/science/article/pii/000527369500117L.

[97] R. J. Mashl, H. L. Scott, S. Subramaniam, and E. Jakobsson, Biophys. J. **81**, 3005 (2001).

[98] Q. Zhu, K. H. Cheng, and M. W. Vaughn, J. Phys. Chem. B **111**, 11021 (2007).

[99] J. B. Lim, B. Rogaski, and J. B. Klauda, J. Phys. Chem. B **116**, 203 (2012).

[100] J. P. M. Jambeck and A. P. Lyubartsev, Phys. Chem. Chem. Phys. **15**, 4677 (2013).

[101] B. D. Madej, I. R. Gould, and R. C. Walker, The Journal of Physical Chemistry B **119**, 12424 (2015).

[102] X. Zhuang, J. R. Makover, W. Im, and J. B. Klauda, Biochimica et Biophysica Acta (BBA) - Biomembranes **1838**, 2520 (2014).

[103] M. Höltje, T. Förster, B. Brandt, T. Engels, W. von Rybinski, and H.-D. Höltje, Biochim. Biophys. Acta **1511**, 156 (2001).

[104] M. T. Hyvönen, T. T. Rantala, and M. Ala-Korpela, Biophys. J. **73**, 2907 (1997).

[105] M. Hyvnen, M. Ala-Korpela, J. Vaara, T. T. Rantala, and J. Jokisaari, Chemical Physics Letters **268**, 55 (1997), ISSN 0009-2614, URL http://www.sciencedirect.com/science/article/pii/S0009261497001711.

[106] S. Feller, D. Yin, R. Pastor, and A. M. Jr, Biophysical Journal **73**, 2269 (1997).

[107] L. Saiz and M. L. Klein, Biophys. J. **204**, 204 (2001).

[108] T. Huber, K. Rajamoorthi, V. F. Kurze, K. Beyer, and M. F. Brown, J. Am. Chem. Soc. **124**, 298 (2002).

[109] S. E. Feller, K. Gawrisch, and A. D. MacKerell Jr., J. Am. Chem. Soc. **124**, 318 (2002).

[110] T. Rg, K. Murzyn, R. Gurbiel, Y. Takaoka, A. Kusumi, and M. Pasenkiewicz-Gierula, Journal of Lipid Research **45**, 326 (2004).

[111] M. T. Hyvönen and P. T. Kovanen, Eur. Biophys. J. **34**, 294 (2005).

[112] J. B. Klauda, V. Monje, T. Kim, and W. Im, The Journal of Physical Chemistry B **116**, 9424 (2012).

[113] W. Kulig, M. Pasenkiewicz-Gierula, and T. Róg, Chem. Phys. Lipids pp. *In Press, Accepted Manuscript, http://dx.doi.org/10.1016/j.chemphyslip.2015.07.002* (2015), URL http://www.sciencedirect.com/science/article/pii/S0009308415300074.

[114] H. I. Petrache, S. W. Dodd, and M. F. Brown, Biophys. J. **79**, 3172 (2000).

[115] K. Rajamoorthi and M. F. Brown, Biochemistry **30**, 4204 (1991).

[116] J. Kapla, B. Stevensson, M. Dahlberg, and A. Maliniak, J. Phys. Chem. B **116**, 244 (2012).

[117] H. Schindler and J. Seelig, Biochemistry **14**, 2283 (1975).

[118] N. V. Eldho, S. E. Feller, S. Tristram-Nagle, I. V. Polozov, and K. Gawrisch, J. Am. Chem. Soc. **125**, 6409 (2003).

[119] W. Stillwell and S. R. Wassall, Chem. Phys. Lipids **126**, 1 (2003).

[120] K. Gawrisch, N. V. Eldho, and L. L. Holte, Lipids **38**, 445 (2003).

[121] J. H. Ipsen, G. Karlstrm, O. Mourtisen, H. Wennerstrm, and M. Zuckermann, Biochimica et Biophysica Acta (BBA) - Biomembranes **905**, 162 (1987).

[122] K. Gawrisch, D. Ruston, J. Zimmerberg, V. Parsegian, R. Rand, and N. Fuller, Biophysical Journal **61**, 1213 (1992).

[123] H. Akutsu and T. Nagamori, Biochemistry **30**, 4510 (1991).

[124] D. J. Semchyschyn and P. M. Macdonald, Magn. Res. Chem. **42**, 89 (2004).

[125] A. Arkhipov, Y. Shan, R. Das, N. Endres, M. Eastwood, D. Wemmer, J. Kuriyan, and D. Shaw, Cell **152**, 557 (2013).

[126] K. Kaszuba, M. Grzybek, A. Orowski, R. Danne, T. Rg, K. Simons, . Coskun, and I. Vattulainen, Proceedings of the Na-

tional Academy of Sciences **112**, 4334 (2015).
[127] G. Lipari and A. Szabo, J. Am. Chem. Soc. **104**, 4546 (1982).
[128] B. Halle and H. Wennerstrm, The Journal of Chemical Physics **75**, 1928 (1981).
[129] A. Nowacka, P. C. Mohr, J. Norrman, R. W. Martin, and D. Topgaard, Langmuir **26**, 16848 (2010).
[130] M. F. Roberts, , and . Alfred G. Redfield*, Journal of the American Chemical Society **126**, 13765 (2004).
[131] M. F. Roberts and A. G. Redfield, Proceedings of the National Academy of Sciences of the United States of America **101**, 17066 (2004).
[132] M. F. Roberts, A. G. Redfield, and U. Mohanty, Biophys. J. **97**, 132 (2009).
[133] E. Lindahl and O. Edholm, J. Chem. Phys. **115**, 4938 (2001).
[134] J. Wohlert, W. K. den Otter, O. Edholm, and W. J. Briels, J. Chem. Phys. **124**, 154905 (2006).
[135] M. Abraham, D. van der Spoel, E. Lindahl, B. Hess, and the GROMACS development team, *GROMACS user manual version 5.0.7* (2015), URL `www.gromacs.org`.
[136] R. Venable, Y. Zhang, B. Hardy, and R. Pastor, Science **262**, 223 (1993).
[137] R. W. Pastor*, , R. M. Venable, and S. E. Feller, Accounts of Chemical Research **35**, 438 (2002).
[138] O. Edholm, in *Computational Modeling of Membrane Bilayers*, edited by S. E. Feller (Academic Press, 2008), vol. 60 of *Current Topics in Membranes*, pp. 91 – 110.
[139] J. B. Klauda, N. V. Eldho, , K. Gawrisch, B. R. Brooks, , and R. W. Pastor*, The Journal of Physical Chemistry B **112**, 5924 (2008).
[140] J. B. Klauda, M. F. Roberts, A. G. Redfield, B. R. Brooks, and R. W. Pastor, Biophysical Journal **94**, 3074 (2008), ISSN 0006-3495, URL `http://www.sciencedirect.com/science/article/pii/S0006349508704648`.
[141] S. E. Feller, D. Huster, , and K. Gawrisch, Journal of the American Chemical Society **121**, 8963 (1999).
[142] M. F. Brown, A. A. Ribeiro, and G. D. Williams, Proceedings of the National Academy of Sciences **80**, 4325 (1983).
[143] A. Nowacka, N. Bongartz, O. Ollila, T. Nylander, and D. Topgaard, Journal of Magnetic Resonance **230**, 165 (2013).
[144] T. M. Ferreira, Ph.D. thesis, Lund University, http://lup.lub.lu.se/record/3878850/file/3879121.pdf (2013).
[145] R. Zhang, R. M. Suter, and J. F. Nagle, Phys Rev E **50**, 5047 (1994).
[146] Y. Lyatskaya, Y. Liu, S. Tristram-Nagle, J. Katsaras, and J. F. Nagle, Phys Rev E **63**, 11907 (2001).
[147] N. Kuerka, Y. Liu, N. Chu, H. I. Petrache, S. Tristram-Nagle, and J. F. Nagle, Biophysical Journal **88**, 2626 (2005).
[148] P. Heftberger, B. Kollmitzer, F. A. Heberle, J. Pan, M. Rappolt, H. Amenitsch, N. Kučerka, J. Katsaras, and G. Pabst, Journal of Applied Crystallography **47**, 173 (2014), URL `24587787`.
[149] N. Kuerka, J. Pencer, J. N. Sachs, J. F. Nagle, and J. Katsaras, Langmuir **23**, 1292 (2007).
[150] N. Kuerka, J. F. Nagle, J. N. Sachs, S. E. Feller, J. Pencer, A. Jackson, and J. Katsaras, Biophysical Journal **95**, 2356 (2008).
[151] V. F. Sears, Neutron News **3**, 26 (1992).
[152] R. W. Benz, F. Castro-Romn, D. J. Tobias, and S. H. White, Biophysical Journal **88**, 805 (2005).
[153] D. T. Cromer and J. B. Mann, Acta Crystallographica Section A **24**, 321 (1968), ISSN 1600-5724, URL `http://dx.doi.org/10.1107/S0567739468000550`.
[154] A. Braun, E. Brandt, O. Edholm, J. Nagle, and J. Sachs, Biophysical Journal **100**, 2112 (2011).
[155] J. Pan, T. T. Mills, S. Tristram-Nagle, and J. F. Nagle, Phys. Rev. Lett. **100**, 198103 (2008).
[156] A. Hodzic, M. Rappolt, H. Amenitsch, P. Laggner, and G. Pabst, Biophysical Journal **94**, 3935 (2008).
[157] N. Kucerka, J. F. Nagle, J. N. Sachs, S. E. Feller, J. Pencer, A. Jackson, and J. Katsaras, Biophys. J. **95**, 2356 (2008), ISSN 0006-3495, URL `http://www.sciencedirect.com/science/article/B94RW-4VB4SVM-S/2/7ede236c4e83d16a6fe57cc3b1894349`.
[158] J. Pan, S. Tristram-Nagle, and J. F. Nagle, Phys. Rev. E **80**, 021931 (2009).
[159] G. Khelashvili, G. Pabst, and D. Harries, The Journal of Physical Chemistry B **114**, 7524 (2010).
[160] (????).
[161] J. N. Sachs, H. I. Petrache, and T. B. Woolf, Chemistry and Physics of Lipids **126**, 211 (2003).
[162] J. B. Klauda, N. Kuerka, B. R. Brooks, R. W. Pastor, and J. F. Nagle, Biophysical Journal **90**, 2796 (2006).
[163] N. Kuerka, J. D. Perlmutter, J. Pan, S. Tristram-Nagle, J. Katsaras, and J. N. Sachs, Biophysical Journal **95**, 2792 (2008).
[164] A. R. Braun, J. N. Sachs, and J. F. Nagle, The Journal of Physical Chemistry B **117**, 5065 (2013).

ToDo